



# Oblique plate convergence along arcuate trenches on a spherical Earth. An example from the Western Sunda Arc

Marco Guzmán-Speziale<sup>1</sup>

Received: 15 November 2019 / Accepted: 24 July 2023 / Published online: 4 September 2023  
© The Author(s) 2023

## Abstract

We propose a new definition of oblique plate convergence. Our model considers arc-trench curvature on a spherical Earth, and defines obliquity as the angle between the direction of plate convergence and the azimuth from the central point along the arc to the center of curvature of the arcuate trench. We also show how this model may be extended to multiple-arc trenches. We apply this definition to the Western Sunda Arc, which has been traditionally considered the prime example of oblique plate convergence, particularly the segment corresponding to Sumatra. We define eight arc-like segments along this arc-trench system. Obliquity angles on these arc-like segments vary from  $92^\circ$  in the northernmost (Burmese) arc to  $7^\circ$  offshore the Sunda strait (between Sumatra and Java). The angle of obliquity offshore Sumatra is  $31^\circ$ , almost within the definition of slightly oblique convergence. Given the low angle of obliquity, partitioning along the Sumatran fault, in the southern portion of the Western Sunda Arc, is difficult to explain by oblique plate convergence alone. We suggest that the entire segment (or forearc) inboard of the Western Sunda Arc be dragged from the Burmese arc, where overriding and subducting plates are completely coupled and oblique plate convergence is high.

**Keywords** Oblique plate convergence · Western Sunda Arc

## Introduction

Harland (1971), proposed that beyond extension, compression and transcurrent relative plate motions, oblique relative movement, such as transtension and transpression, should also be considered. Harland's paper may then be considered as a predecessor in the study of oblique plate convergence. Later, and in a landmark paper, Fitch (1972) proposed that oblique plate convergence yields to a fraction of the slip being transferred to transcurrent motion parallel to the plate margin. Ever since this pioneering work, oblique plate convergence has attracted the attention of workers throughout the Geosciences community.

According to the traditional definition, oblique plate convergence takes place when the angle between the vector of plate convergence and the direction normal to the

trench (the angle of obliquity) differs from zero degrees (e.g., Fitch 1972; Beck 1983; Scotese and Rowley 1985; Curray 1989; Beck 1991; DeMets 1992; McCaffrey 1992; Platt 1993; McCaffrey 1994; Bellier and Sébrier 1995; Jones and Tanner 1995; Teyssier et al. 1995; Liu and McNally 1995; McCaffrey et al. 2000; 2009; Schellart et al. 2011; Díaz-Azpiroz et al. 2016; Bradley et al. 2017; Panda et al. 2018; Ho et al. 2022; Zhang et al. 2022a) (Fig. 1). Scotese and Rowley (1985) classify oblique convergence as: highly oblique (angle of obliquity between  $60^\circ$  and  $90^\circ$ ), moderately oblique ( $30^\circ$ – $60^\circ$ ), and slightly oblique (or nearly orthogonal convergence) ( $0^\circ$ – $30^\circ$ ).

Fitch (1972) and subsequent workers have proposed that oblique plate convergence is generally partitioned into two components: one parallel to slip of thrust-faulting earthquakes along the convergent margin, and another which is resolved parallel to the trench, generally in the form of one or several large strike-slip faults. This is considered the mechanism responsible for detachment and transport of the forearc sliver in many arc-trench systems (Fig. 1).

The basic plane-Earth model of oblique plate convergence (such as the one presented in Fig. 1) is simple: One block represents the plate being subducted along a linear

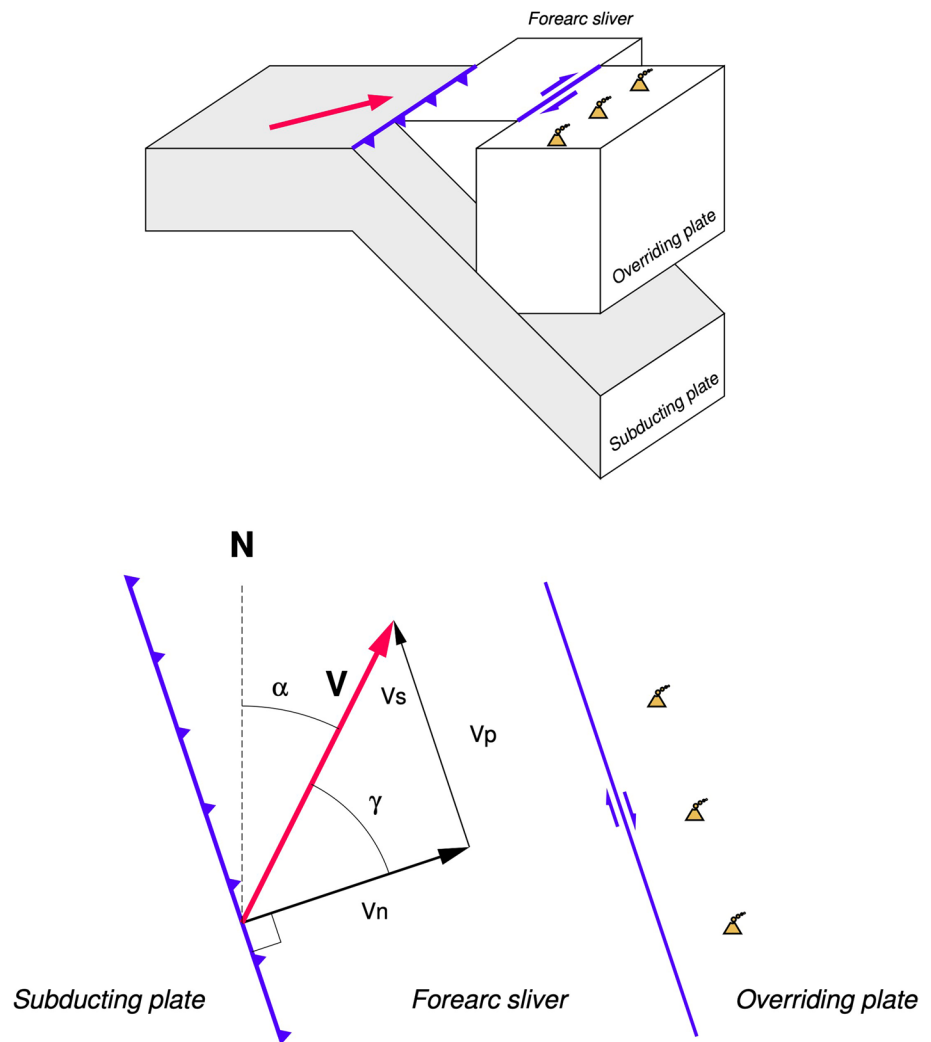
---

Edited by Prof. Ramon Zuñiga (CO-EDITOR-IN-CHIEF).

✉ Marco Guzmán-Speziale  
marco@geociencias.unam.mx

<sup>1</sup> Centro de Geociencias, Universidad Nacional Autónoma de México, Querétaro, México

**Fig. 1** Traditional definition of oblique plate convergence, for a straight trench. **Top.** Block view. **Bottom.** Plan view.  $V$  is plate convergence vector;  $V_n$ , vector normal to trench;  $V_p$ , margin-parallel plate vector.  $\alpha$  is the azimuth of plate convergence and  $\gamma$ , the plate obliquity angle. (Adapted from McCaffrey et al., 2000 and McCaffrey, 2009). All figures were drawn with the help of *The Generic Mapping Tools* software (Wessel and Smith 1991, 1995, 1998; Wessel et al. 2013)



trench. Another block represents the overriding plate. The relative motion between the two plates takes place at an oblique angle  $\gamma$  with respect to the direction normal to the trench. A third block, located between the overriding and subducting plates, and usually called the forearc sliver, is displaced parallel to the trench and along a strike slip fault, because the oblique plate convergence is partitioned between motion perpendicular to the trench and parallel to it (Fig. 1).

This model, with little or no change, has been invoked in published papers throughout the years. As recently as 2023, papers on this subject matter have been published, in which this block model is used throughout. Recent papers span several regions: the Andes (Alvarado et al. 2016; Stanton-Yonge et al. 2016; Catalán et al. 2017; Schütt and Whipp 2020; Seymour et al. 2021; Liu et al. 2023), California (Mookerjee et al. 2016), the Caribbean (Escuder-Viruete and Pérez 2020; Galindo and Lonergan 2020; Bustamante et al. 2021), Central America (Garibaldi et al. 2016), China in the Paleozoic (Hou et al. 2020), Japan (DeMets 1992; Toda et al. 2016), Luzon trough (Zhang et al. 2022b), southern

Mexico (Gaidzik et al. 2016), New Zealand (Guerit et al. 2016), Taiwan (in the Plio-Pleistocene) (Ho et al. 2022), the Western Sunda Arc (Cummins 2007; Kundu and Gahalaut 2012; Berglar et al. 2017; Fernández-Blanco et al. 2016; Bradley et al. 2017; Koulali et al. 2017; Panda et al. 2018; Mallick et al. 2019; Khin et al. 2021; Zhang et al. 2022a; Bose et al. 2023; Wang et al. 2023), the Zagros mountain belt (Malekzade et al. 2016), and world-wide (Philippon and Corti 2016). Other works about analogue (Guerit et al. 2016; Cooke et al. 2020; Schütt and Whipp 2020; Balázs et al. 2021; Jiménez-Bonilla et al. 2022), or numerical modelling (e.g., Platt 1993; Malatesta et al. 2016; Stanton-Yonge et al. 2016; Catalán et al. 2017) also invoke the plane-Earth block model. Many more works published earlier (too many to refer to herein) have also used the same model. Díaz-Azpiroz et al. (2016) (and references therein) present a good review of the literature.

A plane-Earth block model may be suitable for small-scale features, such as the Rosy Finch shear zone in central California (Mookerjee et al. 2016), or El Salvador Fault

System in Central America (Garibaldi et al. 2016) or rupture associated with the 16 April 2016 Kumamoto earthquake in Japan (Toda et al. 2016), but for larger structures, geometrical modelling on a spherical Earth is more appropriate. In this paper, we propose why.

Most, if not all, trenches on Earth are arcuate features, with the shape of an arc (or several) of a small circle (e.g., Frank 1968; Tovish and Schubert 1978; Yamaoka et al. 1986; Yamaoka and Fukao 1987; Guzmán-Speziale 1995; Morra et al. 2006; Mahadevan et al. 2010; Király et al. 2016; Coltice 2023) (Fig. 2).

The direction normal to an arcuate trench on the surface of a spherical Earth is the direction perpendicular to the tangent on the point considered (Fig. 2). This direction is not unique for the entire trench or arcuate segment; in fact, there are as many directions normal to the trench as there are points along it: an infinite number. Consequently, the angles of obliquity along an arcuate trench are also infinite (Fig. 2). McCaffrey (1994) tried to overcome this problem by binning the trench in 75–200 km segments, and calculating trench normal directions to each of these segments. Even then, there will be as many azimuths of trench normal

as there are bins along a given arc-trench system, and the angle of obliquity might even change sign, as in the case of the Mariana or the Peru-Chile trench (Fig. 2).

How can we then define oblique plate convergence along an arcuate trench on a spherical Earth? How is it geometrically possible to transfer slip along an arcuate trench? Is detachment and transport of the forearc block feasible? In this paper, we explore answers to these questions, by proposing a new definition of oblique plate convergence, which takes into account the sphericity of the Earth and the curvature of trenches. We then investigate the role of oblique plate convergence (as defined herein) in detachment and transport of the forearc in the case of the Western Sunda Arc, which has been traditionally considered the prime example of oblique plate convergence and sliver detachment (e.g., Fitch 1972; Newcomb and McCann 1987; Curray 1989; Malod and Kemal 1996; McCaffrey 2009; McNeill and Henstock 2014; Fernández-Blanco et al. 2016; Bradley et al. 2017; Koulali et al. 2017; Panda et al. 2018; Mallick et al. 2019; Khin et al. 2021; Li et al. 2021; Zhang et al. 2022a; Bose et al. 2023; Wang et al. 2023).

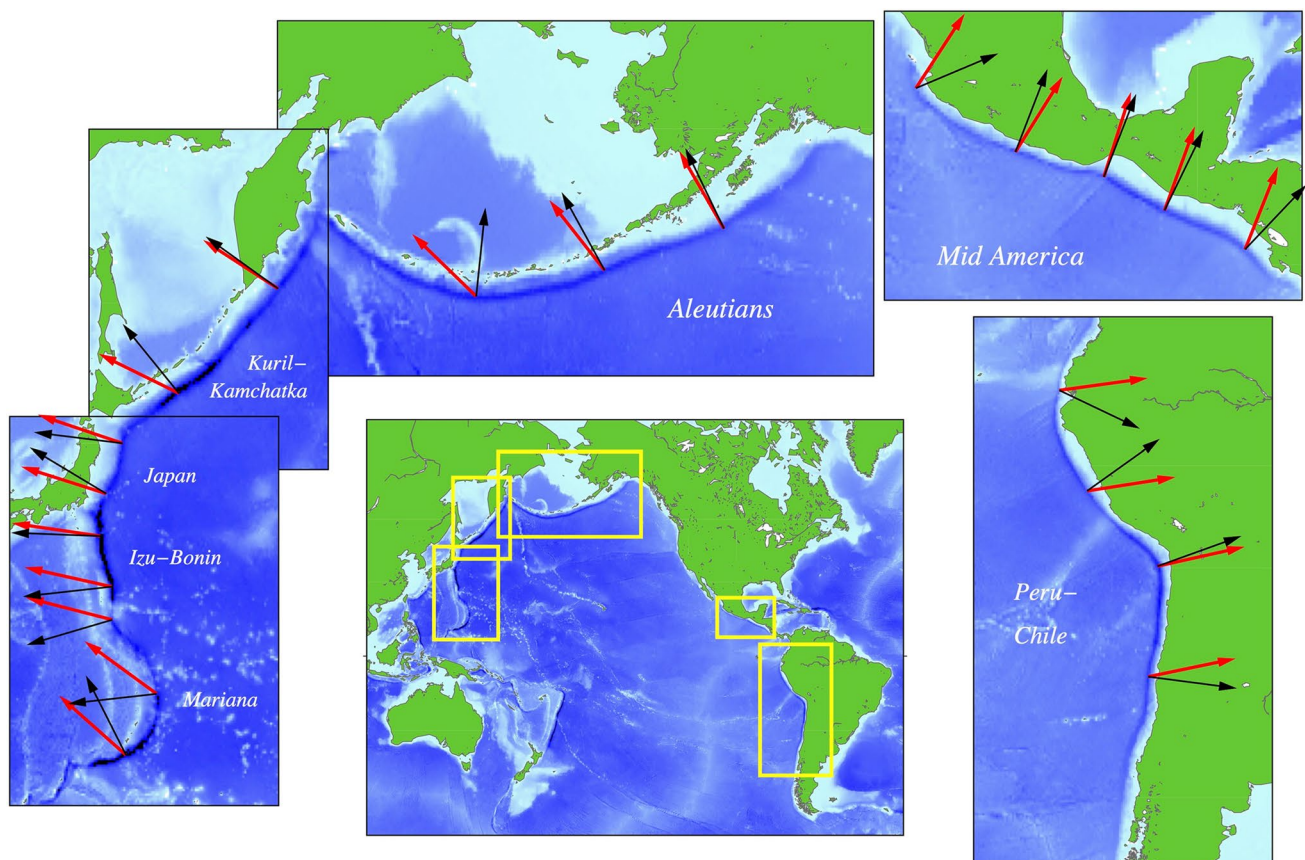


**Fig. 2** Curvature of various arc-trench systems around the Pacific Ocean, showing plate convergence vectors (red arrows) and trench-normal vectors (black arrows). Plate convergence is calculated from

the Euler poles given by DeMets et al. (2010), while trench normal is obtained as the direction perpendicular to the tangent to the trench, at the point considered

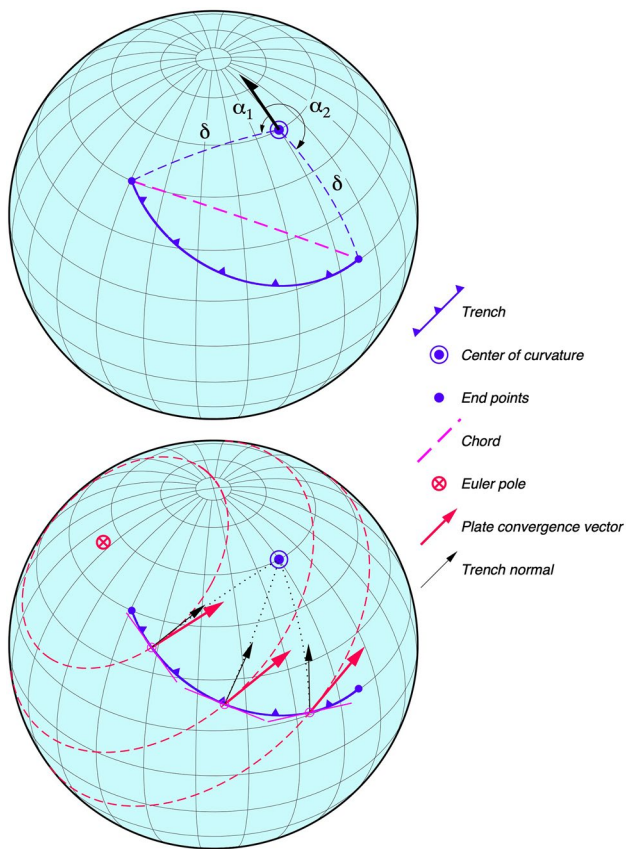


**Fig. 3** **Top.** Parameters of an arcuate trench on a surface of a spherical Earth. The trench is a segment of a small circle on the surface of a spherical Earth. Large half-arrow indicates North. Angular distance  $\delta$  and azimuths  $\alpha$  from center of curvature to end points of the arc are shown. *Chord* is the segment of great circle that joins the end points of the arc. **Bottom.** Plate convergence (red) and trench normal (black) vectors along the arc. Dashed, red lines represent small-circle trajectories around the Euler pole. Plate convergence vectors are tangent to these trajectories. Dotted black lines represent great circles from points along the trench to its center of curvature. Trench-normal vectors are tangent to these great circles. Magenta lines are tangent lines on points (magenta circles) where trench-normal and plate convergence vectors are indicated

### Oblique plate convergence along an arcuate trench on a spherical earth

Consider an arcuate trench consisting of an arc of a small circle on the surface of a spherical Earth (Fig. 3). This arc may be defined by its center of curvature, the angular distance from the center of curvature to the arc  $\delta$ , and by its two end points (which, in turn, may be described by their azimuths  $\alpha_1$  and  $\alpha_2$  from the center of curvature). Additionally, consider the segment of great circle from one end point to the other, i.e., the *chord* between them (Fig. 3).

Relative plate motion between the two plates considered and along the trench is described by rotation around an Euler

pole. Trajectories of motion between the two plates are small circles around the Euler Pole. The direction of plate motion (or plate convergence vector) on a given point along the plate boundary (trench) is the azimuth of the vector tangent to this small circle at this point (Fig. 3).

The direction normal to the trench will be given at each point by the vector perpendicular to the tangent at this particular point. At the same time, this vector will point towards the center of curvature, along a great circle connecting both points (Fig. 3). Obliquity along a trench, in its traditional definition, is the angle between plate convergence direction and trench normal. But in the case of an arcuate trench, and as mentioned above, an infinite number of directions normal to the trench may be obtained (Figs. 2 and 3). Which one defines obliquity of plate convergence?

The vector normal to the trench at the midpoint of the arc is equivalent to taking the average of all directions of trench normal along the arc. This vector is also perpendicular to the chord of the arc (Fig. 4). We propose that this vector may represent the direction normal to the entire arc. Likewise, the angle of obliquity  $\gamma$  will be given by the angle between the vector normal to the trench and the plate convergence vector, both taken at the midpoint of the arc (Fig. 4). In this manner, there will only be one angle of obliquity for the entire arc. The *chord* of the arc is perpendicular to the trench normal (Fig. 4) and is the preferential direction along which strike-slip displacement will most likely take place.

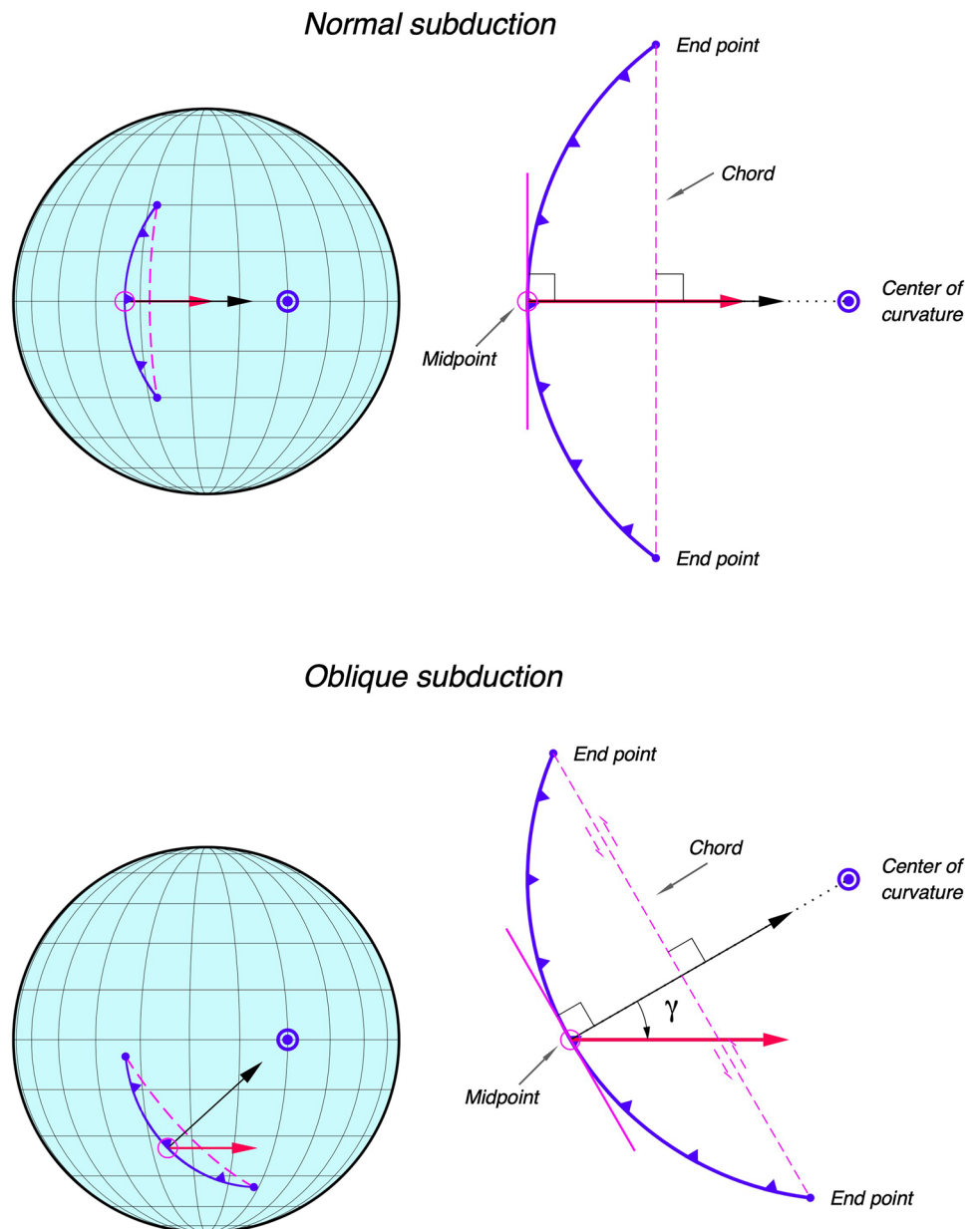
Trenches, however, are usually not composed of one single arc. Most are formed of a small number (usually less than 10) of continuous arc segments (e.g., Frank 1968; Tovish and Schubert 1978; Yamaoka et al. 1986; Yamaoka and Fukao 1987; Guzmán-Speziale 1995; Schellart 2004; Morra et al. 2006; Mahadevan et al. 2010; Li et al. 2021; Coltice 2023). Continuity of the trench means that there are no singular points along it, i.e., at each and every point of the trench there is only one tangent to it. In other words, the curve is continuous and differentiable along its entirety (e.g., Munem and Foulis, 1984). End points of each arcuate segment become points of inflection between neighboring arcs (Fig. 5). Trenches are sometimes joined by cusps (points of singularity) (e.g., Yamaoka and Fukao 1987), such as the Aleutians and Kuril-Kamchatka trenches (Fig. 2), but in this case, they are identified as two different trenches.

The trench will then have as many angles of obliquity as there are arc segments along it (Fig. 5), each determined at the midpoint of its corresponding arc. It might be argued that, in this manner, obliquity could change drastically between adjoining arcs. Usually, however, changes are gradual and subtle. The example of the Western Sunda Arc is shown below.

In order to determine centers of curvature, midpoints, and inflection points along an arc-trench system, it is necessary



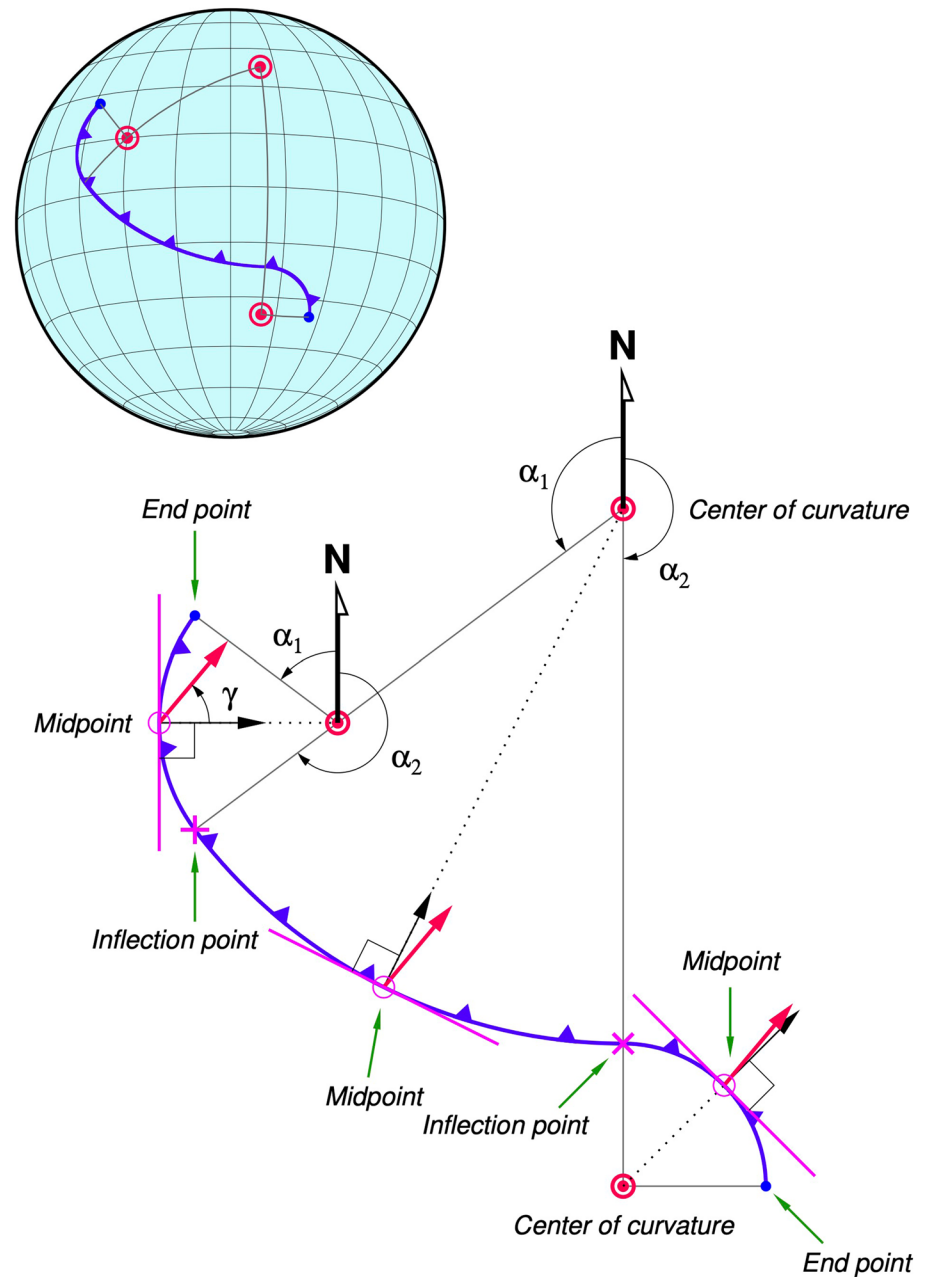
**Fig. 4** *Normal (top)* and *oblique (bottom)* subduction, defined on an arcuate trench. Magenta line on the midpoint is tangent to the arc. All other parameters as defined in Fig. 3. Notice that trench normal for the entire arc is defined at the midpoint as the direction perpendicular to the tangent line. See text for details



first to determine its arcuate segments. This may be achieved using bathymetry data, fitting small circles through the deepest part of the trench and then connecting the resulting circles through their inflection points. Guzmán-Speziale (1995) shows such a procedure for the Mid-America trench, where six arc-segments were adjusted. In summary, the procedure is as follows:

1. Display on a map reliable bathymetric data (e.g., Smith and Sandwell 1997; Becker et al. 2009; Tozer et al. 2019; Fan et al. 2022) for the area of interest.
2. By visual inspection, choose a segment of the trench with constant curvature.
3. Extract data for the deepest part of the arc for this segment.
4. Fit the data to a small circle using, for example, the routine *fitcircle* of *The Generic Mapping Tools* (e.g., Wessel and Smith 1991; Wessel et al. 2013). Guzmán-Speziale (1995) also provides a method to fit a small circle.
5. Repeat step 4 as needed, adding or subtracting points along the trench, until the best fit (in the least-squares sense) is found. This step will also yield the center of curvature of the segment.
6. Repeat steps 2–5 for each identified arc of constant curvature along the trench.
7. Connect arcs so determined by finding their inflection points.

**Fig. 5** Example of an idealized arc-trench system consisting of three arcs. Solid black lines are great circles that connect end- or inflection-points to centers of curvature. Notice that these great circles connect centers of curvature of neighboring segments, and cross the trench at inflection points, even in the case of two adjoining concave segments. Dotted lines are great circles between the midpoint and the center of curvature of the corresponding arc. Other vectors and symbols as in Figs. 3 and 4. **Inset** shows how this trench system would look on a spherical Earth



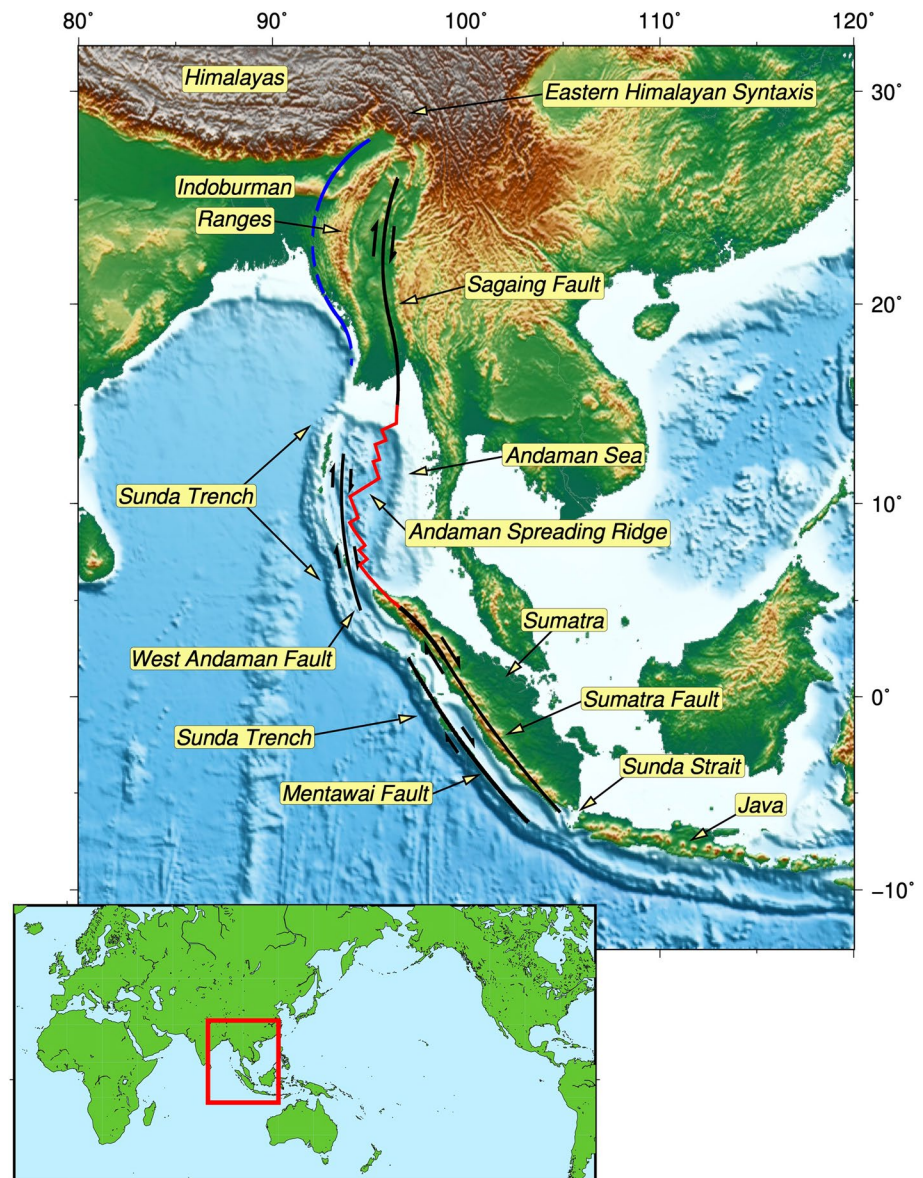
8. Inflection points are found by joining adjacent centers of curvature with a great circle. The inflection point lies on the intersection of both arcs and the great circle (Fig. 5).

With this procedure, the center of curvature of each arc is uniquely determined, the angular distance from it to the arc will be known, as will be the azimuths to the end points (or points of inflection). Centers of curvature

of adjoining segments will lie on the great circle that connects them (Fig. 5). An inflection point between neighboring arcs belongs to both arcs, and is also located on the great circle that connects their centers of curvature (Fig. 5).

In this manner, a few (usually less than 10) segments of adjoining small circles will model an arc-trench system, with

**Fig. 6** Main tectonic elements of the Western Sunda Arc (see text for details). Inset shows location of the arc



their respective centers of curvature. This method reduces the angles of obliquity from an infinite number (Fig. 3) to the number of arcs that form the arc-trench system. The hypothetical trench in Fig. 5 has three arcuate segments (two concave towards subduction, and one convex), each with its center of curvature, middle point, and angle of plate obliquity  $\gamma$ .

This method may also be applied when two adjoining arcs are concave-concave, as shown in Fig. 5. In this case, the centers of curvature of adjoining arcs still lie on a great circle, but they are located on the same side of the trench. A practical example for the Middle America trench can be found in Guzmán-Speziale (1995).

### The Western Sunda Arc

The Western Sunda Arc is an arc-trench system which runs in an approximate N–S to NNW–SSE direction and extends, from north to south, from the Eastern Himalayan Syntaxis to the Sunda Strait (Fig. 6) (e.g., Curray 1989; Guzmán-Speziale and Ni 1996; Bradley et al. 2017; Li et al. 2021; Bose et al. 2023). East of the strait, the arc, although still called the Sunda Arc, takes an E–W orientation and plate convergence is no longer oblique, and therefore beyond the scope of our example. This is the area where Fitch (1972) originally described oblique plate convergence and forearc detachment.

## Main tectonic features

The trench as a physiographic feature along the Western Sunda Arc, shoals from more than 6 km depth off Sumatra to some 3.5 km off the Nicobar Islands (latitude 8°) and finally some 2 km north of the Andaman Islands (latitude ~ 18°) (e.g., Tozer et al. 2019) (Fig. 6). North of this point, the arc is identified by the western foothills of a foreland fold-thrust belt, known by the name of Indoburman ranges (e.g., Mitchell and McKerrow 1975; Bannert et al. 2012), Indo-Burman wedge (Mallick et al. 2019), or Indo-Myanmar ranges (e.g., Khin et al. 2017; 2020; 2022) (Fig. 6). The ranges themselves are thought to be the accretionary wedge, scraped off the subducting Indian Plate, uplifted some 2000 m above sea level. (e.g., Brunnschweiler 1966; Rodolfo 1969; Mitchell 1981; Curray and Lawver 1982; Betka et al. 2018; Khin et al. 2020).

The Sagaing Fault is a right-lateral fault located in the Central Lowlands of Myanmar, east of the Indoburman Ranges (Fig. 6). It extends for about 1200 km. Several authors coincide that total displacement along the fault is in the order of 400–450 km, and has been active in the last 13 Ma, with an average slip rate of 3–3.5 cm/yr (e.g., Curray et al. 1979; Mitchell 1981; Curray and Lawver 1982; Dain et al. 1984; Maung 1987b, a; Vigny et al. 2003; Mallick et al. 2019; Panda et al. 2020; Tin et al. 2022; Fadil et al. 2023; Morishita et al. 2023). This fault takes up at least part of the opening of the Andaman sea (Curray et al. 1979; Guzmán-Speziale and Ni 1993; Kundu and Gahalaut 2012; Steckler et al. 2016; Panda et al. 2020).

On the Andaman Spreading Ridge, sea-floor spreading takes place along a system of east-northeast striking spreading centers that are offset by north-northwest oriented transform faults (e.g., Curray 1989; 2005; Cochran 2010; Srijayanthi et al. 2017; Sagazan and Olive 2021). The extension process has been ongoing for the last 13 Ma, with an average rate of 3.7 cm/yr, as indicated by magnetic anomalies and seismic strain-rate calculations (e.g., Curray et al. 1979; Lawver and Curray 1981; Curray and Lawver 1982; Curray 1989; Guzmán-Speziale and Ni 1993; Radha Krishna and Sanu 2002; Diehl et al. 2013; Kamesh Raju et al. 2020; Jacob et al. 2021; Shamim et al. 2021; Snehashis et al. 2022).

The West Andaman fault, located between the Andaman ridge and the western Sunda arc (Fig. 6), is reported by Curray (1989) as being presently inactive, but taking part in the early opening of the Andaman Sea. McCaffrey (2009) shows the fault as right-lateral. Other workers (e.g., Kamesh Raju et al. 2007; Martin et al. 2014; Snehashis et al. 2022) have found evidence of activity, behaving as a right-lateral, strike-slip structure, although Mahattanachai et al. (2021) suggest that the fault was active only during the Miocene.

The extension process has been ongoing for the last 13 Ma, with an average rate of 3.7 cm/yr, as indicated by magnetic anomalies (e.g., Curray et al. 1979; Lawver and Curray 1981; Curray and Lawver 1982; Curray 1989; Guzmán-Speziale and Ni 1993; Radha Krishna and Sanu 2002).

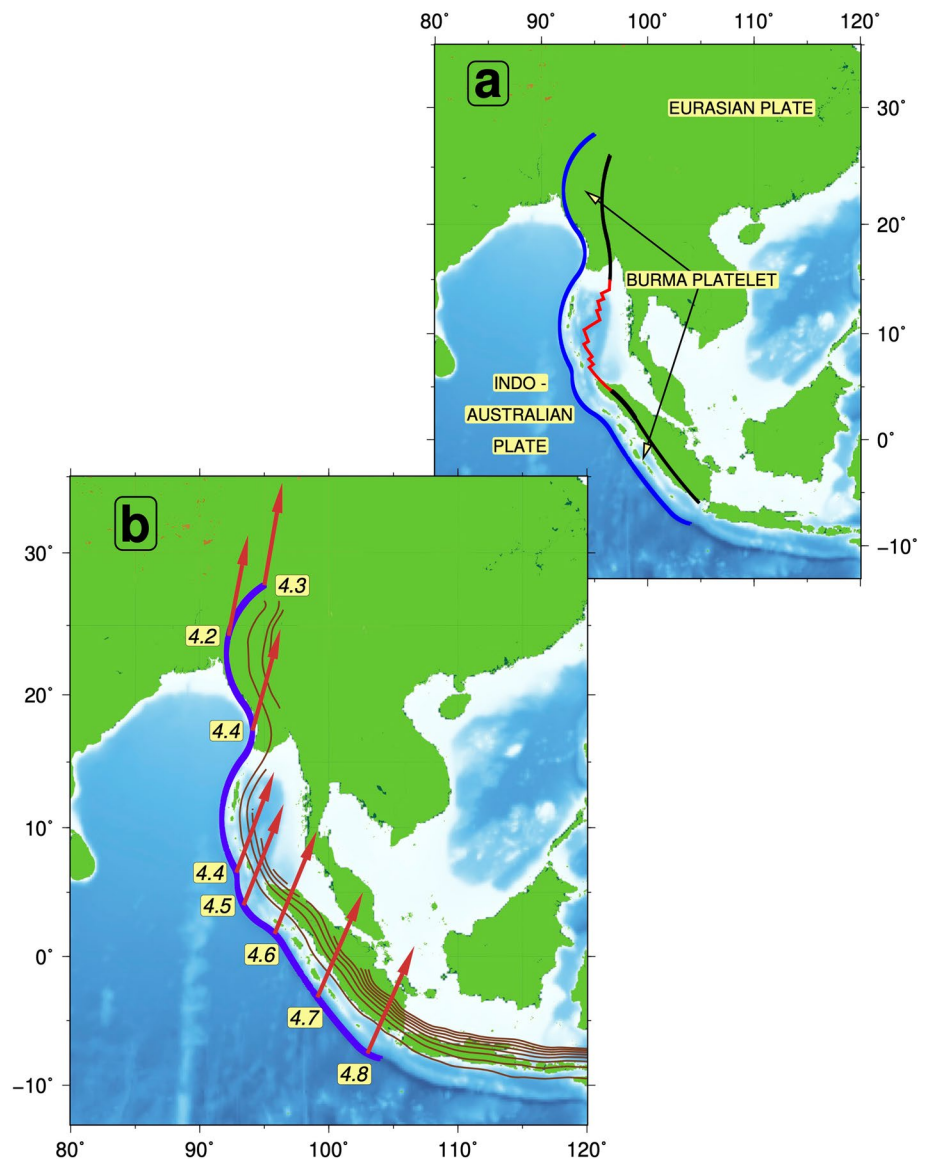
The Sumatra fault, also a right-lateral, strike-slip fault, separates the main overriding plate from the forearc sliver along the volcanic arc of Sumatra (Fig. 6). This is the tectonic feature which Fitch (1972) and other workers afterwards (e.g., Beck 1983; Jarrard 1986; Curray 1989; McCaffrey et al. 2000; McCaffrey 2009; Rafie et al. 2023) have mentioned as case study for oblique plate convergence and slip partitioning. This fault runs along the entire length of the island of Sumatra, for about 1500 km, and along the active volcanic arc (e.g., Siebert et al. 2011; Weller et al. 2012; Rafie et al. 2023). The total offset across the fault is believed to be in the order of 17–23 km (Katili and Hehuwat, 1967; Cameron et al. 1983; Sieh and Natawidjaja 2000; Natawidjaja 2018), although McCarthy and Elders (1997) propose a 150 km offset of Mesozoic units along the Sumatra fault system.

Parallel to the Sumatra fault, closer to the trench, and within the forearc lies the Mentawai fault, a 1200 km long, right-lateral, structure, also active (e.g., Diament et al. 1992; Samuel and Harbury 1996; Sieh and Natawidjaja 2000; Singh et al. 2010; Berglar et al. 2017; Philibosian et al. 2017), although Mukti et al., (2012) and Natawidjaja (2018) regards it as a back thrust (Fig. 6). In fact, Malod and Kemal (1996) and Berglar et al. (2017) consider the area between the Sumatra and Mentawai faults a separate microplate.

Traditionally, it has been considered that the Indo-Australian plate subducts underneath the Eurasian plate along the Sunda trench (e.g., Minster and Jordan 1978; Wiens et al. 1985; DeMets et al. 1990) in a northward direction. Recently, however, a smaller overriding plate has been postulated, which is located between the subducting Indo-Australian plate and the Eurasian plate (the *Burma Plate* of Maung 1987b, a; *Burma platelet* of Guzmán-Speziale and Ni 1996; *Forearc Sliver Plate*, Sieh and Natawidjaja 2000; *Sunda plate* of Bird 2003; *Burma (Myanmar) Plate*, Satyabala 2003; *Burma Plate*, Gahalaut and Gahalaut 2007; *Andaman Microplate*, Engdahl et al. 2007; *Sundaland Plate*, DeMets et al. 2010; *Burmese Microplate*, Akilan et al. 2016; *Myanmar-Andaman-Sumatra Microplate*, Rangin 2016; *Burma sliver*, Panda et al. 2020; *Burma Microplate*, Maneerat et al. 2022), and whose limits are the Sunda trench to the west, the large right-lateral Sagaing and Sumatra faults, together with the Andaman Spreading Ridge to the east (Figs. 6 and 7). According to DeMets et al. (2010), relative motion between the Indo-Australian plate and the Sundaland plate along the arc varies from 4.3 cm/yr at the northernmost end of the convergent margin (next to the Eastern Himalayan Syntaxis),



**Fig. 7** **a** Tectonic plates around the Western Sunda Arc. **b** Relative motion between the Indo-Australian and Burma plates along the Western Sunda Arc, according to the Euler pole given by DeMets et al. (2010) Arrow indicates direction of plate convergence and relative speed (in cm/yr) is given for each point and is proportional to the length of the arrow. Solid brown lines are contour depths of the subducted slab, at 50 km intervals, according to the model of Hayes et al. (2018)



to 4.8 cm/yr along the Sunda trench, offshore the Sunda Strait (Fig. 7).

A subducted slab has been clearly identified throughout the arc, from the Eastern Himalayan Syntaxis to the Sunda strait (e.g., Guzmán-Speziale and Ni 1996; Satyabala 1998; Gahalaut et al. 2013; Kundu and Gahalaut 2013; Steckler et al., 2016; Hayes et al. 2018; Mallick et al. 2019; Khin et al. 2021), even though there are no interplate earthquakes along the northernmost part of the arc (e.g., Guzmán-Speziale and Ni 1996, 2000; Satyabala 1998).

That is why, Guzmán-Speziale and Ni (1996) consider the Sunda arc-trench system to extend to the Eastern Himalayan Syntaxis. We follow them here.

## Seismicity

Essentially, all of the tectonic features of the Western Sunda arc, are seismically active (e.g., Newcomb and McCann 1987; Guzmán-Speziale and Ni 1996; Hurukawa and Maung Maung 2011; Hurukawa et al. 2014; Feng et al. 2015; Kumar et al. 2015; Carter and Bandopadhyay 2017; Salman et al. 2020; Hutchings and Mooney 2021; Srivastava et al. 2021) (Fig. 8).

Seismic activity along the Sagaing fault has been reported by Le Dain et al., (1984), Molnar and Deng (1984), Vigny et al. (2003) (Fig. 8). Several large earthquakes have occurred along the fault in 1908 ( $M=7.5$ ), 1912 ( $M=8$ ), two in 1930 ( $M=7.3$ , both), 1931 ( $M=7.6$ ), 1946 ( $M=7.75$ ), 1956 ( $M=7.0$ ) (Molnar and Deng 1984;

**Fig. 8** Seismicity of the Western Sunda Arc. Data from the ISC-EHB catalogue (1964–2019) (Engdahl, et al. 1998; Weston et al. 2018; International Seismological Centre 2023) and the United States Geological Survey (USGS) catalogue (2020–2023) (<https://www.usgs.gov/programs/earthquake-hazards>). **a** Epicenters for shallow ( $z \leq 50$  km) events (light gray circles – events with depths shallower than 25 km; dark-gray circles, events with depths between 25 and 50 km). Magnitudes between 4.0 and 7.0. **b** Same as a), but for events with magnitudes equal or larger than 7.0. **c** Epicenters for intermediate depth ( $50 \text{ km} < z \leq 80$  km; orange symbols) and deep ( $z > 80$  km; red symbols) events. Larger symbols indicate earthquakes with magnitude 7.0 or greater

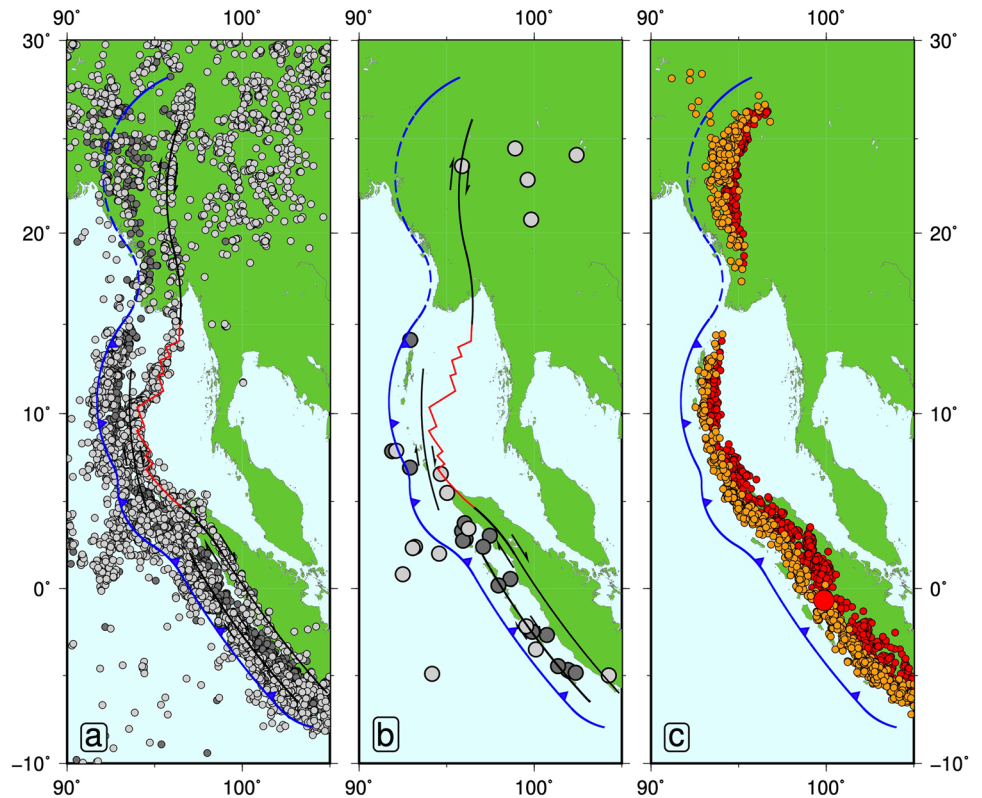
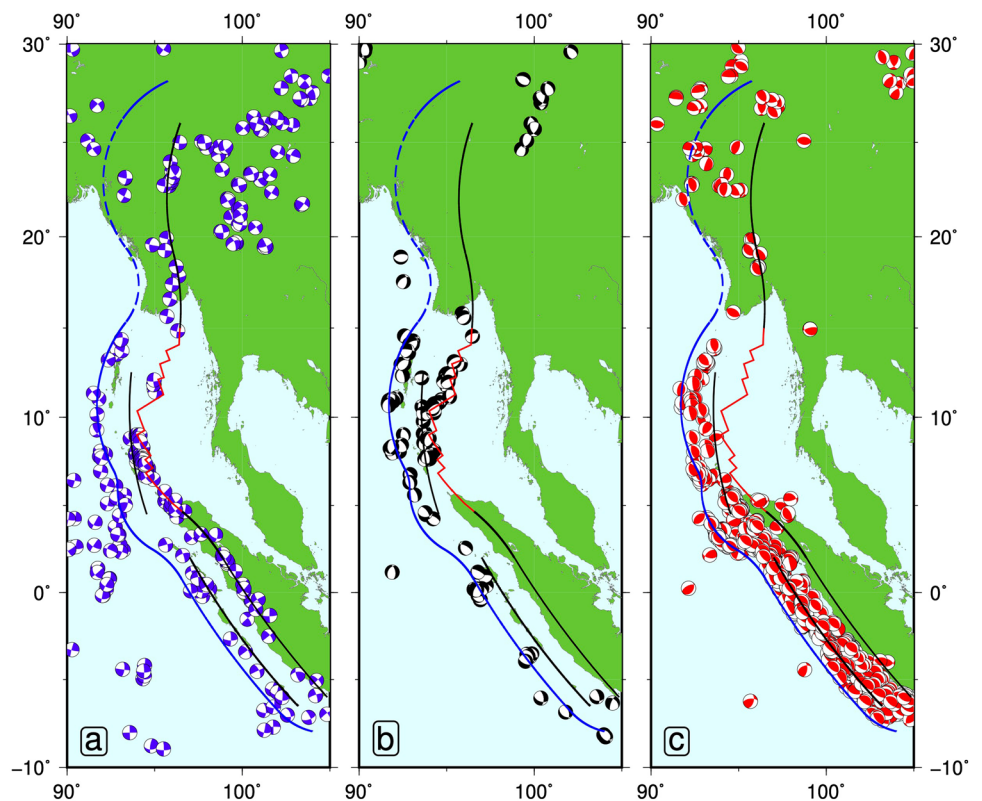


**Fig. 9** Earthquake focal mechanisms for shallow ( $z \leq 25$  km) earthquakes in the Western Sunda Arc. **a** Strike-slip events; **b** Normal-faulting events; **c** Thrust-faulting events



Vigny et al. 2003; Tsutsumi and Sato 2009; Hurukawa and Maung Maung; 2011). More recently, the ISC-EHB catalog (Engdahl et al. 1998, 2020; Weston et al. 2018; International Seismological Centre 2023) catalog lists one large earthquake ( $M=7.0$ ) along this fault in 1991. Earthquakes with magnitudes  $M < 7.0$  have also been reported along the fault (e.g., ISC-EHB catalog). Available focal mechanisms (e.g., Le Dain et al. 1984; Guzmán-Speziale and Ni 1996; Global Centroid-Moment Tensor (CMT) Project (<http://www.globa lcmt.org>)) show right-lateral, strike-slip faulting along the fault (Fig. 9). Additional faults adjacent to the Sagaing are also seismically active, such as the Churachandpur Mao fault (e.g., Kundu and Gahalaut 2013; Tiwari et al. 2015) or the Kopili fault (Singh et al. 2017). GPS results show a slip rate of 16–24 mm/yr along this fault (Maurin et al. 2010; Tin et al. 2022).

The Andaman Sea (Fig. 6), is the site of shallow earthquakes (Fig. 8), both right-lateral, strike-slip faulting and normal-faulting (Fig. 9) (e.g., Rajendran and Gupta 1989; Dasgupta and Mukhopadhyay 1993; Guzmán-Speziale and Ni 1996; Carter and Bandopadhyay 2017; Singha et al. 2019; Srijayanthi and Ravi Kumar 2020; Bhat et al. 2021; Shamin et al., 2021; Jacob et al. 2021; International Seismological Centre 2023). They are associated with the Andaman

Spreading Ridge, where sea-floor spreading takes place along a system of east-northeast striking spreading centers that are offset by north-northwest oriented transform faults (e.g., Curray 1989; Guzmán-Speziale and Ni 1993; 1996; Srijayanthi et al. 2017). There is also shallow seismicity along the West Andaman and Mentawai faults (Fig. 8), with strike-slip, right-lateral seismic mechanisms (e.g., Global CMT project).

The Sumatra fault is seismically active (Figs. 8 and 9). Engdahl and Villaseñor (2002) report seven large ( $M \geq 7.0$ ), shallow ( $z \leq 50$  km) earthquakes on or near the Sumatra fault which could be related to activity along the fault: 1900 ( $M=7.0$ ), 1909 ( $M=7.2$ ), 1917 ( $M=7.1$ ), 1933 ( $M=7.3$ ), 1935 ( $M=7.0$ ), 1936 ( $M=7.1$ ), two in 1943 ( $M=7.2$  and  $M=7.5$ ), and 1946 ( $M=7.1$ ). Focal mechanisms of earthquakes along the Sumatra fault are generally right-lateral, strike-slip (e.g., Sukmono et al. 1997; Weller et al. 2012; Jacob et al. 2021; Global CMT project). The right-lateral Mentawai fault is also seismically active (Fig. 8 and 9) (Lasitha et al. 2006; Mukti et al. 2012; Weller et al. 2012; Syafriani 2018).

It is well known that the southern portion of the western Sunda Arc is the site of very large interplate earthquakes, such as the 26 December, 2004 event ( $M_w 9.1$ ), the 28

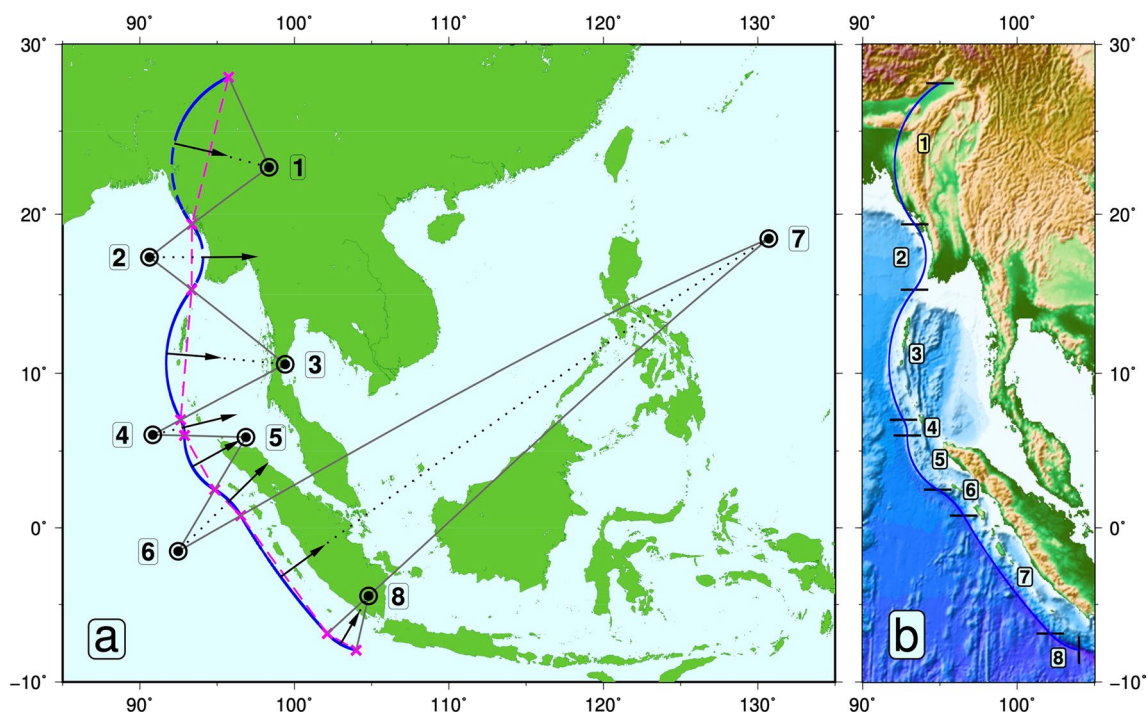


**Fig. 10** Arc-like segments along the Western Sunda Arc. **a** Eight segments along the arc. Centers of curvature of their respective arcs are numbered circles. Magenta crosses are inflection points. Dashed lines are the chords of the arcs. Notice that centers of curvature of adjoining arcs are linked by a great circle (solid line in this map projection).

Arrows are trench normal vectors; they start at mid point of their corresponding arc and point to the center of curvature (dotted line). **b** Topography and bathymetry of the Western Sunda Arc is shown, for reference, along with the eight segments of the arc. See text for details



March, 2005 quake ( $M_w = 8.6$ ) (e.g., Engdahl et al. 2007), or the 12 September, 2007 event ( $M_w = 8.5$ ) (e.g., Konca et al. 2008). Other great earthquakes ( $M \geq 8$ ) have also been identified throughout the historic record, in 1797, 1833, and 1861 along the southern arc (Newcomb and McCann 1987; Sieh and Natawidjaja 2000; Natawidjaja et al. 2006; Engdahl et al. 2007). Somewhat smaller ( $M < 8$ ), but significant, thrust-faulting events in the historic record have been identified in the central part of the arc, in 1847, 1881, and 1941 (Bilham et al. 2005). On the other hand, interplate events are practically absent in the northern part of the arc, north of about latitude  $15^\circ$  (Fig. 8), right where the trench loses its physiographic signal (e.g., Guzmán-Speziale and Ni 1996, 2000; Satyabala 1998; Gahalaut et al. 2013; Mukhopadhyay et al. 2016). Large outer-arc strike-slip earthquakes also take place (Fig. 9); worth mentioning is the 2012 doublet ( $M_w = 8.6$  and  $M_w = 8.2$ ; Duputel et al. 2012).

Although there is no physical trench in the northern part of the arc, a Wadati-Benioff zone can be traced throughout the entire arc, except for the northern Andaman sea (between latitudes  $14^\circ$  and  $17^\circ$ , approximately) (Figs. 7 and 8) (e.g., Ni et al. 1989; Guzmán-Speziale and Ni 1996; Satyabala 1998; 2003; Khan 2005; Hurukawa et al. 2012; Gahalaut et al. 2013; Hayes et al. 2018; Bhat et al. 2021). Earthquake hypocenters usually reach a depth of no more than 200–220 km in the south (Sumatra–Andaman arc) and about 150 km in the Burmese arc, in the north. Fault-plane solutions within the subducted slab show thrust-faulting, normal-faulting, and strike-slip mechanisms, all with **P** axes parallel to the trench, which Guzmán-Speziale and Ni (1996) interpreted this as a compressive state of stress parallel to the arc (in the N–S direction) and tension perpendicular to it (and parallel to the direction of maximum slope).

GPS results (e.g., Chamot-Rooke and Le Pichon 1999; Michel et al. 2000, 2001; Socquet et al. 2006; Simons et al. 2007; Chlieh et al. 2008; Gahalaut et al. 2013; Singh et al. 2014; Mallick et al. 2019) confirm that the *Burma, Sunda*, or

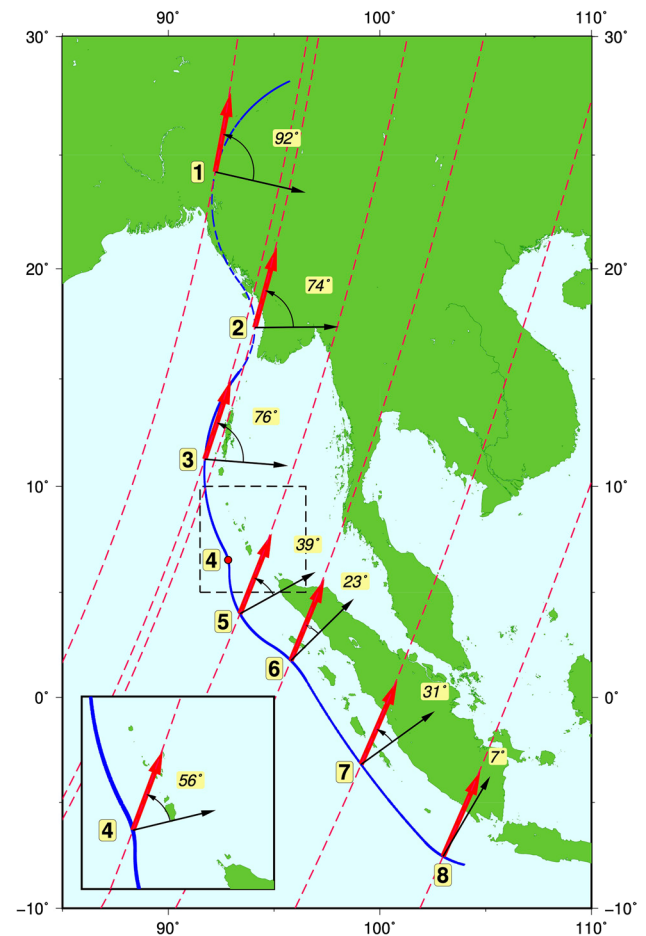


**Fig. 11** Obliquity angles for the eight arc-like segments along the Western Sunda Arc. Red arrows indicate the direction of plate convergence between the India and Sundaland plates (DeMets et al. 2010) in the mid points of each arc. Black arrows are the direction of trench normal for each of the arcs, as determined in this work (see Fig. 10 and Table 1). Small-circle trajectories around the India-Sundaland Euler pole are shown as dashed red lines. The small circle, plate convergence and trench normal vectors for arc 4 are shown in the inset, for clarity

**Table 1** Parameters of the eight arc-like segments along the Western Sunda Arc

N	C	$\delta^\circ$	IP	MP	FP	TN
1	22.85°–98.36°	5.80	28.15°–95.74°	24.27°–92.22°	19.38°–93.37°	102.93°
2	17.35°–90.62°	3.31	19.38°–93.37°	17.35°–94.09°	15.32°–93.35°	89.47°
3	10.58°–99.40°	7.57	15.32°–93.35°	11.28°–91.73°	7.03°–92.64°	94.56°
4	6.05°–90.84°	2.04	7.03°–92.64°	6.53°–92.83	6.01°–92.89°	76.25°
5	5.90°–96.86°	3.95	6.01°–92.89°	3.98°–93.39°	2.49°–94.85°	60.91°
6	–1.53°–92.48°	4.66	2.49°–94.85°	1.75°–95.79°	0.80°–96.52°	45.29°
7	18.50°–130.71°	37.92	0.80°–96.52°	–3.19°–99.11°	–6.88°–102.13°	53.93°
8	–4.44°–104.81°	3.61	–6.88°–102.13°	–7.56°–102.99°	–7.96°–104.00°	30.20°

N, Number; C, Center of curvature (latitude, longitude);  $\delta$ , Distance from center of curvature to arc (in degrees); IP, Initial (northernmost) point of segment (latitude, longitude); MP, Mid point of segment (latitude, longitude); FP, Final (southernmost) point of segment (latitude, longitude). TN, azimuth of trench normal, in degrees



**Table 2** Angles of obliquity in mid-points along the Western Sunda Arc

N	Lat	Lon	$\alpha$	$\gamma$
1	24.27	92.22	10.93	92.00
2	17.35	94.09	15.23	74.24
3	11.28	91.73	18.14	76.42
4	6.53	92.83	20.43	55.82
5	3.98	93.39	21.51	39.40
6	1.75	95.79	22.13	23.16
7	-3.19	99.11	23.22	30.71
8	-7.56	102.99	23.47	6.73

Angles are calculated for the India-Sundaland *Euler* pole of DeMets et al. [2010]. *Lat.*, *Lon.*, is the location of the midpoint of the arc;  $\alpha$  is the azimuth of plate convergence;  $\gamma$  is the angle of obliquity

*Sundaland* platelet is being displaced to the North-Northeast with respect to Eurasia.

### Arc-geometry and oblique plate convergence in the western Sunda arc

Following the procedure described above in Sect. "Oblique plate convergence along an arcuate trench on a spherical earth", we fit eight arc-like (small circle) segments to the Western Sunda Arc (Fig. 10). Arcs three through eight are fitted to the deepest part of the trench, while arc two was fitted to the 2000 m depth contour. Finally, arc one was determined parallel to the trend of the Indoburman Ranges and continuous from the other arcs, because, there is no active trench associated to it (e.g., Guzmán-Speziale and Ni 1996; Gahalaut et al. 2013). Table 1 lists the parameters of each of the eight segments identified here: Location of centers of curvatures, initial, mid, and end points, as well as distance from the center of curvature to the arc (in degrees) and the azimuth of trench normal. From segments one to seven, centers of curvature are located alternatively to the East and West of the Western Sunda Arc. That is, arcs are alternatively concave and convex, with respect to the overriding Burma plate. The center of curvature for segment eight is located on the same (concave) side as that of segment seven (Fig. 10).

Trench normal direction is the azimuth from the midpoint to the center of curvature, in the case of segments 1, 3, 5, 7, and 8 (concave segments), and the azimuth from the center of curvature to the midpoint for segments 2, 4, and 6 (convex segments) (Fig. 10). Only in the case of arc one is the azimuth of trench normal somewhat arbitrary, because it depends on the location of the northernmost end point of the arc, not determined by an actual trench (Fig. 10; Table 1). Arcs one through four are oriented roughly in a N–S direction, which is readily evident from Fig. 10, and also from the

azimuth of trench normal, which is close to 90° (Table 1). Arcs five through eight are oriented in a more NW–SE direction (Fig. 10; Table 1).

We determine obliquity along the WSA using the pole of rotation of the Indian plate with respect to Sundaland of DeMets et al. (2010). This *Euler* pole is located at latitude  $-21.2^\circ$  and longitude  $-151.8^\circ$ , with an angular velocity of 0.444 deg/myr. As stated above, the angle of obliquity for each arcuate segment is the difference between the azimuth of plate convergence and the direction normal to the trench at the mid point of each arc (Fig. 11; Table 2).

Angles of plate obliquity along the WSA determined by India-Sundaland relative plate motion range from 92° along the Burmese arc (northernmost portion of the arc), to 31° offshore Sumatra, and finally 7° along segment eight (Fig. 11; Table 2). According to the classification of Scotese and Rowley (1985), convergence along arcs one, two, and three is highly oblique (92°, 74°, and 76°, respectively), moderate along arcs four (56°), five (39°), and seven (31°) and slight along segment six (23°) and eight (7°) (Table 2; Fig. 11).

### Discussion

Few, if any, arc trench systems are a straight line (or, equivalently, a great circle on the surface of a spherical Earth): perhaps the southern part of the Perú-Chile (Fig. 2) or the Tonga-Kermadec trench, in the southwestern Pacific Ocean approximate this geometry.

Flat-Earth models with straight trenches are well suited for small sections of the Earth, spanning only a few kilometers. Determining oblique convergence on a point-by-point basis along a straight trench may be justifiable for such models. But using them for entire arc-trench systems that can stretch for hundreds of kilometers, in a succession of connecting arc-like features on an almost spherical Earth may lead to problems. As seen on Fig. 2, point-by-point determination of obliquity angles leads to significant differences in the angles, and even abrupt changes of sign.

The idea of an arcuate trench is not new (e.g., Frank 1968; Tovish and Schubert 1978; Hsui and Youngquist 1985; Yamaoka et al. 1986; Yamaoka and Fukao 1987; Morra et al. 2006; Mahadevan et al. 2010; Boutelier and Cruden 2013; Cramer and Tackley 2014; Király et al. 2016), nor is the method of dividing the trench into several adjoining arc-like segments (Guzmán-Speziale 1995). However, oblique plate convergence on a spherical Earth with arcuate trenches had not been fully explored in the past.

Here, we present a new approach to the problem of oblique plate convergence on a spherical Earth. We fit the

trench to a small number of continuous, arc-like features, either concave or convex towards subduction (e.g., Guzmán-Speziale 1995), and assign a trench normal to each one of the segments, from the central point of the arc and in the direction of the center of curvature of the arc. This is equivalent to taking the average of plate normal for each and every point along the arcuate segment. The angle of obliquity, between trench normal and plate convergence vector, may then be calculated uniquely for each of the arcs (Fig. 5), as the difference between the azimuth of plate convergence and the azimuth of the trench-normal vector.

We use the Western Sunda Arc (WSA) as an example for our proposed model, because of the high obliquity of convergence between the Indian and the Burma plates along it (e.g., Fitch 1972; Beck 1983; Curray 1989; Guzmán-Speziale and Ni 1996; Bradley et al. 2017; Acocella et al. 2018). In fact this is the place where oblique plate convergence was first recognized (Fitch 1972).

Eight continuous arc-like segments are fitted to the entire trench, from the Eastern Himalayan Syntaxis, to the Sunda Strait. The three northernmost arcs are oriented approximately in a N–S direction, as determined by their chord and/or by their orthogonal trench-normal vector (Table 1; Fig. 10), while the rest are oriented NW–SE.

Relative motion between the Indian and Sundaland plates is determined using the Euler pole proposed by DeMets et al. (2010). Obliquity along the arc is then calculated for each of the eight arcs, as the difference between the vector of India-Sundaland plate convergence, and the trench-normal vector, at the central point of each of the arcs. Obliquity along the WSA ranges from  $92^\circ$  along the Burmese arc, to  $7^\circ$  in front of the Sunda strait (Table 2; Fig. 11).

The idea set forward by Fitch (1972), that oblique plate convergence offshore Sumatra is responsible for decoupling of slip on the western Sunda region, leading to right-lateral motion along the Sumatra fault, has prevailed ever since. Results presented here suggest that oblique plate convergence is more pronounced along the three northernmost arcs, north of about latitude  $7^\circ$  N (latitude of the northernmost tip of the island of Sumatra) (Fig. 11). In the classification of Scotese and Rowley (1985), arcs one, two, and three along the northernmost Western Sunda Arc are under high oblique plate convergence ( $92^\circ$ ,  $74^\circ$ , and  $76^\circ$ , respectively), whereas the southern section (arcs four to eight), with an obliquity average of  $25^\circ$ , is only slightly oblique (see also Table 2 and Fig. 11).

What then, triggers slip partitioning and right-lateral, strike-slip deformation along the Sumatra fault? Obliquity of  $31^\circ$  along much of Sumatra (segment seven) (Table 2; Fig. 11) may indeed be a contributing factor, but let us consider oblique plate convergence along the entire Western Sunda Arc.

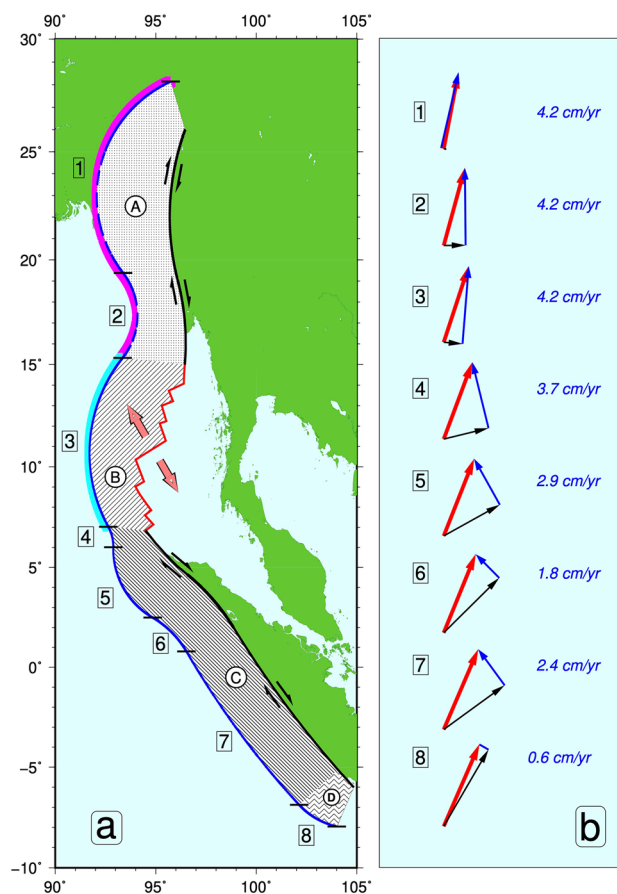


**Fig. 12** Model for oblique plate convergence along the Western Sunda Arc. **a** Areas of the Burma platelet. A- locked (coupled) area, represented by thick purple line along the trench. B- extension area (light blue along the trench). C- Forearc slip area. D- Transition area. **b** Velocity vector diagrams for arcs along the Western Sunda Arc. Red arrow is plate convergence vector; black arrow, trench normal vector; blue arrow, chord-parallel velocity component. The value of this component (speed) is also indicated

Along the northern part (arcs one and two in this work), a well-defined Wadati-Benioff zone has been clearly delineated (e.g., Ni et al. 1989; Guzmán-Speziale and Ni 1996; Satyabala 1998; Gahalaut et al. 2013; Kundu and Gahalaut 2013; Steckler et al., 2016), but there are no thrust-faulting, shallow interplate earthquakes. This led Guzmán-Speziale and Ni (1996) to propose that active plate convergence (*sensu stricto*) has ceased from the Eastern Himalayan syntaxis to about latitude  $15^\circ$  (arcs one and two in this work) and that the plate boundary is strongly coupled.

The India-Sundaland plate boundary is then most probably strongly coupled, or even locked, along arcs one and two, although Mallick et al. (2019) report a great ( $M \sim 8$ ) thrust earthquake that took place in the Arakan area in 1762. South of latitude  $15^\circ$  (arc three) there are thrust-faulting, interplate earthquakes (Fig. 9) (Guzmán-Speziale and Ni 1996). As suggested by Ni et al. (1989), Gahalaut and Gahalaut

(2007), and Khin et al. (2020), this probably resulted in the mechanical dragging of the Sundaland (Burma) platelet to the north-northeast. Coupling of the two plates, on the other hand, may have been the consequence of high oblique plate convergence (cf., Scotese and Rowley 1985). In other words, the northern Sundaland platelet is *trapped* by highly oblique plate convergence and by the arcuate shape of arc one (e.g., Ni et al. 1989). Khin et al. (2020) argue that, "... the Burma Plate was wedged in the subduction zone and dragged towards the north with the Indian Plate between internal N–S trending right-lateral shearing and external E–W shortening."

The rest of the platelet is probably being dragged along to the NNW, resulting in the opening of the Andaman spreading ridge, where a thinner oceanic crust could facilitate the process, and right-lateral, strike-slip faulting along the Sumatra fault.

Figure 12 shows a schematic model of the process: Area **A**, which comprises arcs one and two, is locked at the trench, at least temporarily. At the same time, it is the zone where the highest oblique plate convergence takes place, with a margin-parallel vector oriented almost in a N–S direction and a component of speed of 4.2 cm/yr (Fig. 12). This leads to right-lateral, strike-slip deformation along the Sagaing fault. Area **B** (arc three) corresponds to rifting of the oceanic crust along the Andaman spreading ridge. Plate convergence is still highly oblique and its trench-parallel component is still 4.2 cm/yr (Fig. 12). Area **C** is characterized by smaller trench-parallel velocities: from 3.7, 2.9, 1.8, and 2.4 cm/yr in arcs four through seven, with an average of 2.7 cm/yr. These vectors are oriented in a more NW–SE direction (Fig. 12). Finally, area **D** is the transition between the western and the rest of the Sunda Arc, and is characterized by a very small (0.6 cm/yr) trench parallel component (Fig. 12).

Trench-parallel components calculated here are in good agreement with results presented elsewhere: Mallick et al. (2019) use GPS techniques to estimate a total north–south shear in the Burma (Myanmar) area of about 30 mm/yr, with the Sagaing fault taking up 20 mm/yr, compared to the 42 mm/yr calculated herein. Acocella et al. (2018) report a geologic slip across the Sumatra fault of 2.7–0.68 cm/yr, decreasing from north to south, a geodetic slip of 2.3–2.6 cm/yr, and a trench-parallel component of 2.9 cm/yr.

Even though tectonic plates are generally considered rigid (at least in the short term), the process described above must lead to internal stretching of the Sundaland (Burma) platelet. Several authors propose that, indeed, the interior of this platelet is in tension, noticeable as rifting along the Andaman Sea (e.g., Guzmán-Speziale and Ni 1993; 1996), and decreasing slip rates along the Sumatra fault, from north to south (e.g., McCaffrey 1991; 1992; Bellier and Sébrier 1995; Genrich et al. 2000; McCaffrey et al. 2000; Mukhopadhyay

et al. 2016; Bradley et al. 2017; Acocella et al. 2018), thus supporting the model presented here.

## Conclusions

A new way to define oblique plate convergence is presented here. It is based on fitting an arc-trench system with contiguous and continuous segments of small circles. Trench-normal direction of each arc is calculated at the mid-point of every arc only. Azimuth of trench normal vector is also the direction from the mid point of the arc to its center of curvature. Obliquity of plate convergence is the angular difference between the plate convergence vector and the trench normal vector, both at the mid point of each arc. Trench parallel velocity vector is a chord-parallel vector.

This new definition is applied to the Western Sunda Arc, where eight segments are fitted, and obliquity of plate convergence is calculated. The largest obliquity is found along the three northernmost segments, where obliquity is high and the subducting and overriding plates seem to be completely coupled. Offshore Sumatra, obliquity is low, and apparently coupling is low. This suggests that oblique plate convergence along the northern Western Sunda Arc, together with plate coupling, is dragging the Sundaland platelet to the north-northeast, causing right-lateral, strike-slip faulting along the great Sagaing and Sumatra faults (and probably the Mentawai and West Andaman faults also), as well as opening of the Andaman spreading ridge.

**Acknowledgements** Discussion with several colleagues of *Centro de Geociencias* and *Instituto de Geofísica*, both *UNAM*, resulted in improvements of the ideas presented herein. Carlos Mendoza thoroughly read the manuscript and made many valuable comments. Manuel Díaz-Azpiroz critically read an earlier version of the manuscript and made comments that greatly improved it. Two anonymous reviewers also made very valuable remarks. I also thank Dr. F. Ramón Zúñiga, co-editor-in-chief, for his patience. *Centro de Geociencias*, *UNAM* contribution 2009.

## Declarations

**Conflict of interest** The corresponding author (sole author of this work) states that there is no conflict of interest.

**Open Access** This article is licensed under a Creative Commons Attribution 4.0 International License, which permits use, sharing, adaptation, distribution and reproduction in any medium or format, as long as you give appropriate credit to the original author(s) and the source, provide a link to the Creative Commons licence, and indicate if changes were made. The images or other third party material in this article are included in the article's Creative Commons licence, unless indicated otherwise in a credit line to the material. If material is not included in the article's Creative Commons licence and your intended use is not permitted by statutory regulation or exceeds the permitted use, you will

need to obtain permission directly from the copyright holder. To view a copy of this licence, visit <http://creativecommons.org/licenses/by/4.0/>.

## References

- Acocella V, Bellier O, Sandri L, Sébrier M, Pramumijoyo S (2018) Weak tectono-magmatic relationships along an obliquely convergent plate boundary: Sumatra Indonesia. *Front Earth Sci*. <https://doi.org/10.3389/feart.2018.00003>
- Akilan A, Balaji S, Padhy S, Abdul Azeez KK, Srinivas Y (2016) The plate kinematics of Burmese micro-plate relative to its surroundings. *Arab J Geosci* 9:333. <https://doi.org/10.1007/s12517-016-2345-6>
- Alvarado A, Audin L, Nocquet JM, Jaillard E, Mothes P, Jarrín P, Segovia M, Rolandone F (2016) Partitioning of oblique convergence in the Northern Andes subduction zone: migration history and the present-day boundary of the North Andean sliver in Ecuador. *Tectonics* 35:1048–1065. <https://doi.org/10.1002/2016TC004117>
- Balázs A, Faccenna C, Ueda K, Funicello F, Boutoux A, Blanc EJ-P, Gerya T (2021) Oblique subduction and mantle flow control on upper plate deformation: 3D geodynamic modeling. *Earth Planet Sci Lett* 569:117056. <https://doi.org/10.1016/j.epsl.2021.117056>
- Bannert D, Sang Lyen A, Htay T (2012) The geology of the Indoburman ranges in Myanmar. *Geologisches Jahrbuch, Reihe B, Heft, Hannover*, p 101
- Beck ME (1983) On the mechanism of tectonic transport in zones of oblique subduction. *Tectonophysics* 93:1–11
- Beck ME (1991) Coastwise transport reconsidered: lateral displacements in oblique subduction zones, and tectonic consequences. *Phys Earth Planet Inter* 68:1–8
- Becker JJ, Sandwell DT, Smith WHF, Braud J, Binder B, Depner J, Fabre D, Factor J, Ingalls S, Kim S-H, Ladner R, Marks K, Nelson S, Pharaoh A, Trimmer R, Von Rosenberg J, Wallace G, Weatherall P (2009) Global bathymetry and elevation data at 30 arc seconds resolution: SRTM30\_PLUS. *Mar Geod* 32(4):355–371. <https://doi.org/10.1080/01490410903297766>
- Bellier O, Sébrier M (1995) Is the slip rate variation on the great Sumatran fault accommodated by forearc stretching? *Geophys Res Lett* 22:1969–1972
- Berglar K, Gaedicke C, Ladage S, Thöle H (2017) The Mentawai forearc sliver off Sumatra: a model for a strike-slip duplex at a regional scale. *Tectonophysics* 710–711:225–231. <https://doi.org/10.1016/j.tecto.2016.09.014>
- Betka PM, Seeber L, Thomson SN, Steckler MS, Sincavage R, Zoramathara C (2018) Slip-partitioning above a shallow, weak décollement beneath the Indo-Burman accretionary prism. *Earth Planet Sci Lett* 503:17–28. <https://doi.org/10.1016/j.epsl.2018.09.003>
- Bhat GR, Iqbal V, Yousuf M, Wani S (2021) Seismotectonics and spatio-temporal variations in seismicity rates along Andaman trench. *J Geol Soc India* 97:249–254. <https://doi.org/10.1007/s12594-021-1674-6>
- Bilham R, Engdahl ER, Feldl N, Satyabala P (2005) Partial and complete rupture of the Indo-Andaman plate boundary 1847–2004. *Seismol Res Lett* 76:299–311
- Bird P (2003) An updated digital model of plate boundaries. *Geochem Geophys Geosyst* 4:1–52
- Bose S, Schellart WP, Strak V, Duarte JC, Chen Z (2023) Sunda subduction drives ongoing India-Asia convergence. *Tectonophysics* 849:229727. <https://doi.org/10.1016/j.tecto.2023.229727>
- Boutelier D, Cruden A (2013) Slab rollback rate and trench curvature controlled by arc deformation. *Geology* 41:911–914. <https://doi.org/10.1130/G343338.1>
- Bradley KE, Feng L, Hill EM, Natawidjaja DH, Sieh K (2017) Implications of the diffuse deformation of the Indian Ocean lithosphere for slip partitioning of oblique plate convergence in Sumatra. *J Geophys Res* 122:572–591. <https://doi.org/10.1002/2016JB013549>
- Brunnschweiler RO (1966) On the geology of the Indoburman ranges (Arakan coast and Yoma, Chin hills, Naga hills). *J Geol Soc Aust* 13:137–194
- Bustamante C, Archanjo CJ, Cardona A, Restrepo M (2021) Magnetic fabric of the Parashi stock and related dyke swarm, Alta Guajira (Colombia): the Caribbean-South American plates oblique convergence. *Andean Geol* 48:219–236. <https://doi.org/10.5027/andgeoV48n2-3332>
- Cameron N, Clarke M, Aldiss D, Aspoden J, Djunuddin, A (1983) The geological evolution of northern Sumatra. In: *Proceedings, 9th Indonesian petroleum association annual convention, Jakarta*
- Carter A, Bandopadhyay PC (2017) Seismicity of the Andaman-Nicobar Islands and Andaman sea, in Bandopadhyay, P. C. and Carter, A. (editors) *The Andaman-Nicobar Accretionary Ridge: Geology, Tectonics and Hazards*. *Geol Soc Lond Mem* 47:205–213. <https://doi.org/10.1144/M47.14>
- Catalán N, Bataille K, Tassara A, Araya R (2017) Depth-dependent geometry of margin-parallel strike-slip faults within oblique subduction zones. *Andean Geol* 44:79–86
- Chamot-Rooke N, Le Pichon X (1999) GPS determined eastward Sundaland motion with respect to Eurasia confirmed by earthquakes slip vectors at Sunda and Philippine trenches. *Earth Planet Sci Lett* 173:439–455
- Chlieh M, Avouac JP, Sieh K, Natawidjaja DH, Galetzka J (2008) Heterogeneous coupling of the Sumatran megathrust constrained by geodetic and paleogeodetic measurements. *J Geophys Res* 113:B05305. <https://doi.org/10.1029/2007JB004981>
- Cochran JR (2010) Morphology and tectonics of the Andaman forearc, Northeastern Indian ocean. *Geophys J Int* 182:631–651
- Coltice N (2023) Tectonics is a hologram. In: Duarte JC (ed) *Dynamics of plate tectonics and mantle convection*. Elsevier, Netherlands, pp 105–125
- Cooke ML, Toeneboehn K, Hatch JL (2020) Onset of slip partitioning under oblique convergence within scaled physical experiments. *Geosphere* 16(3):875–889. <https://doi.org/10.1130/GES02179.1>
- Cramer F, Tackley PJ (2014) Spontaneous development of arcuate single-sided subduction in global 3-D mantle convection models with a free surface. *J Geophys Res Solid Earth* 119:5921–5942. <https://doi.org/10.1002/2014JB010939>
- Cummins PR (2007) The potential for giant tsunamigenic earthquakes in the northern Bay of Bengal. *Nature* 449:75–78. <https://doi.org/10.1038/nature06088>
- Curry JR (1989) The Sunda arc: a model for oblique plate convergence. *Neth J Sea Res* 24:131–140
- Curry JR (2005) Tectonics and history of the Andaman sea region. *J Asian Earth Sci* 25:187–232
- Curry JR, Moore DG, Lawver LA, Emmel FJ, Raitt RW, Henry M, Kieckhefer RM (1979) Tectonics of the Andaman sea and Burma, in *Geological and Geophysical Investigations of Continental Margins*, edited by J. Watkins, L. Montadert, and P. W. Dickerson. *Am Assoc Pet Geol Mem* 29:189–198
- Curry JR, Lawver LA (1982). The Andaman sea- a ripoff type of backarc basin. In: *Geodynamics of back-arc regions symposium*, Texas A&M University, College Station, TX, vol 29. p. 30
- Le Dain AY, Tapponnier P, Molnar P (1984) Active faulting and tectonics of Burma and surrounding regions. *J Geophys Res* 89:453–472
- Dasgupta S, Mukhopadhyay M (1993) Seismicity and plate deformation below the Andaman arc, Northeastern Indian ocean. *Tectonophysics* 225:529–542. [https://doi.org/10.1016/0040-1951\(93\)90314-A](https://doi.org/10.1016/0040-1951(93)90314-A)



- DeMets C (1992) Oblique convergence along the Kuril and Japan trenches. *J Geophys Res* B12:17615–17625. <https://doi.org/10.1029/92JB01306>
- DeMets C, Gordon RG, Argus DF (2010) Geologically current plate motions. *Geophys J Int* 181:1–80
- DeMets C, Gordon RG, Argus DF, Stein S (1990) Current plate motions. *Geophys J Int* 101:425–478
- Diament M, Harjono H, Karta K, Deplus C, Dahrin D, Zen MT, Gérard M, Lassal O, Martin A, Malod J (1992) Mentawai fault zone off Sumatra: a new key to the geodynamics of western Indonesia. *Geology* 20:259–262
- Diehl T, Waldhauser F, Cochran JR, Kamesh Raju KA, Seeber L, Schaff D, Engdahl ER (2013) Back-arc extension in the Andaman sea: tectonic and magmatic processes imaged by high-precision teleseismic double-difference earthquake relocation. *J Geophys Res* 118:2206–2224. <https://doi.org/10.1002/jgrb.50192>
- Duputel Z, Kanamori H, Tsai VC, Rivera L, Meng L, Amouero J-P, Stock JM (2012) The 2012 Sumatra great earthquake sequence. *Earth Planet Sci Lett* 351–352:247–257. <https://doi.org/10.1016/j.epsl.2012.07.017>
- Díaz-Azpiroz M, Brune S, Leever K, Fernández C, Czeck DM (2016) Tectonics of oblique plate boundary systems. *Tectonophysics* 693:165–170
- Engdahl ER, Di Giacomo D, Sakarya B, Gkarlaoui CG, Harris J, Storchak DA (2020) ISC-EHB 1964–2016, an improved data set for studies of earth structure and global seismicity. *Earth Space Sci.* <https://doi.org/10.1029/2019EA000897>
- Engdahl ER, van der Hilst R, Buland R (1998) Global teleseismic earthquake relocation with improved travel times and procedures for depth determination. *Bull Seismol Soc Am* 88:722–743
- Engdahl ER, Villasenor A (2002) Global seismicity: 1900–1999. In: Lee HK, Kanamori H, Jennings PC et al (eds) *International handbook of earthquake and engineering seismology*, part A. Academic Press, Amsterdam
- Engdahl ER, Villaseñor A, DeShon HR, Thurber CH (2007) Teleseismic relocation and assessment of seismicity (1918–2005) in the region of the 2004 Mw 9.0 Sumatra-Andaman and 2005 Mw 8.6 Nias Island great earthquakes. *Bull Seismol Soc Am* 97:S43–S61. <https://doi.org/10.1785/0120050614>
- Escuder-Viruete J, Pérez Y (2020) Neotectonic structures and stress fields associated with oblique collision and forearc sliver formation in northern Hispaniola: implications for the seismic hazard assessment. *Tectonophysics* 784:228452. <https://doi.org/10.1016/j.tecto.2020.228452>
- Fadil W, Wei S, Bradley K, Wang Y, He Y, Sandvol E, Huang B-S, Hubbard J, Thant M, Htwe Y (2023) Active faults revealed and new constraints on their seismogenic depth from a high-resolution regional focal mechanism catalog in Myanmar (2016–2021). *Bull Seismol Soc Am* 113:613–635. <https://doi.org/10.1785/0120220195>
- Fan D, Li S, Feng J, Sun Y, Xu Z, Huang Z (2022) A new global bathymetry model: STO\_IEU2020. *Remote Sens* 14:5744. <https://doi.org/10.3390/rs14225744>
- Feng L, Hill EM, Banerjee P, Hermawan I, Tsang LLH, Natawidjaja DH, Suwargadi BW, Sieh K (2015) A unified GPS-based earthquake catalog for the Sumatran plate boundary between 2002 and 2013. *J Geophys Res* 120:3566–3598. <https://doi.org/10.1002/2014JB011661>
- Fernández-Blanco D, Philippon M, von Hagke C (2016) Structure and kinematics of the Sumatran fault system in North Sumatra (Indonesia). *Tectonophysics* 693:453–464
- Fitch TJ (1972) Plate convergence, transcurrent faults, and internal deformation adjacent to Southeast Asia and the Western Pacific. *J Geophys Res* 77:4432–4460
- Frank F (1968) Curvature of island arcs. *Nature* 220:363. <https://doi.org/10.1038/220363a0>
- Gahalaut VK, Gahalaut K (2007) Burma plate motion. *J Geophys Res* 112:B10402. <https://doi.org/10.1029/2007JB004928>
- Gahalaut V, Kundu B, Laishram SS, Catherine J, Kumar A, Singh MD, Tiwari RP, Chadha RK, Samanta SK, Ambikapathy A, Mahesh P, Bansal A, Narsaiah M (2013) Aseismic plate boundary in the Indo-Burmese wedge, northwest Sunda Arc. *Geology* 41:235–238
- Gaidzik K, Ramírez-Herrera MT, Kostoglodov V (2016) Active crustal faults in the forearc region, Guerrero sector of the Mexican subduction zone. *Pure Appl Geophys* 173:3419–3443
- Galindo PA, Lonergan L (2020) Basin evolution and shale tectonics on an obliquely convergent margin: the Bahia Basin, offshore Colombian Caribbean. *Tectonics*. <https://doi.org/10.1029/2019TC005787>
- Garibaldi N, Tikoff B, Hernández W (2016) Neotectonic deformation within an extensional stepover in El Salvador magmatic arc, Central America: implication for the interaction of arc magmatism and deformation. *Tectonophysics* 693:327–339
- Genrich JF, Bock Y, McCaffrey R, Prawirodirdjo L, Stevens CW, Puntodewo SSO, Subarya C, Wdowinski S (2000) Distribution of slip at the northern Sumatran fault system. *J Geophys Res* 105:28327–28341. <https://doi.org/10.1029/2000JB900158>
- Guerit I, Domínguez S, Malavieille J, Castellort S (2016) Deformation of an experimental drainage network in oblique collision. *Tectonophysics* 693:210–222
- Guzmán-Speziale M (1995) Hypocentral cross-sections and arc-trench curvature. *Geofísica Internacional* 34:131–141
- Guzmán-Speziale M, Ni JF (1993) (1993), The opening of the Andaman sea: Where is the short-term displacement being taken up? *Geophys Res Lett* 20:2949–2952
- Guzmán-Speziale M, Ni JF (2000) Comment on “subduction in the Indo-Burma region’ Is it still active?” by S. P. Satyabala. *Geophys Res Lett* 27:1065–1066. <https://doi.org/10.1029/1999GL005428>
- Guzmán-Speziale M, Ni JF (1996) Seismicity and active tectonics of the western Sunda arc. In: Yin A, Mark Harrison T (eds) *The tectonic evolution of Asia*. Cambridge University Press, New York, pp 63–84
- Harland WB (1971) Tectonic transpression in Caledonian Spitsbergen. *Geol Mag* 108:27–49
- Hayes G, Moore GL, Portner D, E., Hearne, M., Flamme, H., Furtney, M., Smoczyk, G. M. (2018) Slab2, a comprehensive subduction zone geometry model. *Science* 362:58–61. <https://doi.org/10.1126/science.aat4723>
- Ho G-R, Byrne T, Lee J-C, Mesalles L, Lin C-W, Lo W, Chang CP (2022) A new interpretation of the metamorphic core in the Taiwan orogen: A regional-scale, left-lateral shear zone that accommodated highly oblique plate convergence in the plio-pleistocene. *Tectonophysics* 833:229332. <https://doi.org/10.1016/j.tecto.2022.229332>
- Hou L, Zhang C, Lin Y, Li C, Huang Y, Dong T, Wu H (2020) From oblique arc-continent collision to orthogonal plate subduction in the southeastern central Asia orogenic belt during paleozoic: evidence from superimposed folds at the northern margin of the north China craton. *J Asian Earth Sci* 200:104499. <https://doi.org/10.1016/j.jseas.2020.104499>
- Hsui A, Youngquist S (1985) A dynamic model of the curvature of the Mariana trench. *Nature* 318:455–457. <https://doi.org/10.1038/318455a0>
- Hurukawa N, Maung Maung P (2011) Two seismic gaps on the Sagaing Fault, Myanmar, derived from relocation of historical earthquakes since 1918. *Geophys Res Lett* 38:L01310. <https://doi.org/10.1029/2010GL046099>
- Hurukawa N, Tun PP, Shibazaki B (2012) Detailed geometry of the subducting Indian plate beneath the Burma plate and subcrustal

- seismicity in the Burma plate derived from joint hypocenter relocation. *Earth Planets Space* 64:333–343
- Hurukawa N, Wulandari BR, Kasahara M (2014) Earthquake history of the Sumatran fault, Indonesia, since 1892, derived from relocation of large earthquakes. *Bull Seismol Soc Am* 104:1750–1762. <https://doi.org/10.1785/0120130201>
- Hutchings SJ, Mooney WD (2021) The seismicity of Indonesia and tectonic implications. *Geochem Geophys Geosyst*. <https://doi.org/10.1029/2021GC009812>
- International seismological centre (2023), ISC-EHB dataset, <https://doi.org/10.31905/PY08W6S3>
- Jacob J, Dymant J, Ghosal D, Dewangan P (2021) Strike-slip seismicity at the Andaman-Sumatra subduction zone: role of the fracture zones and age of the subducting lithosphere. *Tectonophysics* 811:228862. <https://doi.org/10.1016/j.tecto.2021.228862>
- Jarrard RD (1986) Terrane motion by strike-slip faulting of forearc slivers. *Geology* 14:780–783
- Jiménez-Bonilla A, Ramos IE, Díaz-Azpíroz M, Balnyá JC, Crespo-Blanc, A. (2022) Strain partitioning and localization due to detachment heterogeneities in fold-and-thrust belts of progressive arcs: results from analog modeling. *Tectonics*. <https://doi.org/10.1029/2021TC006955>
- Jones RR, Tanner PWG (1995) Strain partitioning in transpressional zones. *J Struct Geol* 17:793–802
- Kamesh Raju KA, Aswini KK, Yatheesh V (2020) Tectonics of the Andaman backarc basin—present understanding and some outstanding questions. In: Ray Jyotirajan S, Radhakrishna M (eds) *The Andaman Islands and adjoining offshore: geology, tectonics and palaeoclimate*. Springer, Cham, pp 237–259. [https://doi.org/10.1007/978-3-030-39843-9\\_12](https://doi.org/10.1007/978-3-030-39843-9_12)
- Kamesh Raju KA, Murty GPS, Amamath D, Mohan Kumar ML (2007) The west Andaman fault and its influence on the after-shock pattern of the recent megathrust earthquakes in the Andaman-Sumatra region. *Geophys Res Lett* 34:L03305. <https://doi.org/10.1029/2006GL028730>
- Katili J, Huhuwat F (1967) On the occurrence of large transcurrent faults in Sumatra Indonesia. *J Geosci Osaka City Univ* 10:5–17
- Khan PK (2005) Variation in dip-angle of the Indian plate subducting beneath the Burma plate and its tectonic implications. *Geosci J* 3:227–234
- Khin K, Moe A, Aung KP (2022) Tectono-structural framework of the Indo-Myanmar ranges: implications for the structural development on the geology of the Rakhine coastal region, Myanmar. *Geosyst Geoenviron* 1:100079. <https://doi.org/10.1016/j.geogeo.2022.100079>
- Khin K, Moe A, Myint M (2020) Geology, structure and lithostratigraphic framework of the Rakhine coastal ranges in western Myanmar: implications for the collision of the India plate and west Myanmar block. *J Earth Sci* 196:104332
- Khin K, Moe A, Myint M, Aung KP (2021) Dextral transpressional shearing and strike-slip partitioning developments in the central Myanmar basin during the collision between the India plate and west Myanmar block. *J Asian Earth Sci* X 5:100055. <https://doi.org/10.1016/j.jaesx.2021.100055>
- Khin K, Zaw K, Aung LT (2017) Geological and tectonic evolution of the Indo-Myanmar ranges (IMR) in the Myanmar region, in Barber, A. J., Khin Zaw, Crow, M. J. (editors), *Myanmar: Geology Resources and Tectonics*. *Geol Soc Lond Mem* 48:65–79. <https://doi.org/10.1144/M48.4>
- Király A, Capitano F, Funicicello F, Faccena C (2016) Subduction zone interaction: controls on arcuate belts. *Geology* 44:715–718. <https://doi.org/10.1130/G37912.1>
- Konca A, Avouac JP, Sladen A, Meltzner A J, Sieh K, Fang P, Li Z, Galetzka J, Genrich J, Chlieh M, Natawidjaja D, Bock Y, Fielding EJ, Ji C, Helmberger D (2008) Partial rupture of a locked patch of the Sumatra megathrust during the 2007 earthquake sequence. *Nature* 456:631–635. <https://doi.org/10.1038/nature07572>
- Koulali A, McClusky S, Susilo S, Leonard Y, Cummins P, Tregoning P, Meilano I, Efendi J, Wijanarto AB (2017) The kinematics of crustal deformation in Java from GPS observations: implications for fault slip partitioning. *Earth Planet Sci Lett* 458:69–79
- Kumar A, Mitra S, Suresh G (2015) Seismotectonics of the eastern Himalayan and Indo-Burman plate boundary systems. *Tectonics* 34:2279–2295. <https://doi.org/10.1002/2015TC003979>
- Kundu B, Gahalaut VK (2012) Earthquake occurrence processes in the Indo-Burmese wedge and Sagaing fault region. *Tectonophysics* 524–525:135–136
- Kundu B, Gahalaut VK (2013) Tectonic geodesy revealing geodynamic complexity of the Indo-Burmese arc region North East India. *Curr Sci* 104:920–933
- Lasitha S, Radhakrishna M, Sanu TD (2006) Seismically active deformation in the Sumatra-Java trench-arc region: geodynamic implications. *Curr Sci* 90:690–696
- Lawver LA, Curray JR (1981) Evolution of the Andaman sea. *EOS* 62:1044
- Li J, Ding W, Lin J, Xu Y, Kong F, Li S, Huang X, Zhou Z (2021) Dynamic processes of the curved subduction system in south-east Asia: A review and future perspective. *Earth Sci Rev* 217:103647. <https://doi.org/10.1016/j.earscirev.2021.103647>
- Liu H, Liu L, Zhang D, Huang F, Zhang X (2023) Unilateral magma emplacement of the Telimbela batholith in the central Ecuadorian arc: implications for kinematics of oblique subduction of the Farallon-Nazca plate. *Tectonics*. <https://doi.org/10.1029/2021TC007114>
- Liu X, McNally K (1995) Evidence for a role of the downgoing slab in earthquake slip partitioning at oblique subduction zones. *J Geophys Res* 100:15351–15372
- Mahadevan L, Bendick R, Liang H (2010) Why subduction zones are curved. *Tectonics*. <https://doi.org/10.1029/2010TC002720>
- Mahattanachai T, Morley CK, Charusiri P, Kanjanapayont P (2021) The Andaman basin central fault zone, Andaman sea: characteristics of a major deepwater strike-slip fault system in a polyphase rift. *Mar Pet Geol* 128:104997. <https://doi.org/10.1016/j.marpetgeo.2021.104997>
- Malatesta C, Gerya T, Crispini L, Federico L, Capponi G (2016) Interplate deformation at early-stage oblique subduction: 3-D thermomechanical numerical modeling. *Tectonics* 35:1610–1625. <https://doi.org/10.1002/2016TC004139>
- Malekzade Z, Bellier O, Abbassi MR, Shabaniyan E, Authemayou C (2016) The effects of plate margin inhomogeneity on the deformation pattern within west-central Zagros fold-and-thrust belt. *Tectonophysics* 693:304–326
- Mallick R, Lindsey EO, Feng L, Hubbard J, Banerjee P, Hill EM (2019) Active convergence of the India-Burma-Sunda plates revealed by a new continuous GPS network. *J Geophys Res* 124:3155–3171. <https://doi.org/10.1029/2018JB016480>
- Malod JA, Kemal BM (1996) The Sumatra margin: oblique subduction and lateral displacement of the accretionary prism. *Geol Soc Lond Spec Publ* 106:19–28. <https://doi.org/10.1144/GSL.SP.1996.106.01.03>
- Maneerat P, Dreger DS, Bürgmann R (2022) Stress orientations and driving forces in the Indo-Burma plate boundary zone. *Bull Seismol Soc Am* 112:1323–1335. <https://doi.org/10.1785/0120210303>
- Martin KM, Gulick SPS, Austin JA, Berglar K, Franke D (2014) The west Andaman fault: a complex strain-partitioning boundary at the seaward edge of the Aceh Basin, offshore Sumatra. *Tectonics* 33(5):786–806. <https://doi.org/10.1002/2013TC003475>

- Maung H (1987a) Transcurrent movements in the Burma-Andaman sea region. *Geology* 15:911–912
- Maung H (1987b) Transcurrent movements in the Burma-Andaman sea region. *Geology* 15:911–912
- Maurin T, Masson F, Rangin CT, Min U, Collard P (2010) First global positioning system results in northern Myanmar: constant and localized slip rate along the Sagaing fault. *Geology* 38:591–594. <https://doi.org/10.1130/G30872.1>
- McCaffrey R (1991) Slip vectors and stretching of the Sumatran forearc. *Geology* 19:881–884
- McCaffrey R (1992) Oblique plate convergence, slip vectors, and forearc deformation. *J Geophys Res* 97:8905–8915
- McCaffrey R (1994) Global variability in subduction thrust zone-forearc systems. *Pure Appl Geophys* 142:173–224
- McCaffrey R (2009) The tectonic framework of the Sumatran subduction zone. *Annu Rev Earth Planet Sci* 37:345–366
- McCaffrey R, Zwick PC, Bock Y, Prawirodirdjo L, Genrich JF, Stevens CW, Puntodewo SSO, Subarya C (2000) Strain partitioning during oblique plate convergence in northern Sumatra; geodetic and seismologic constraints and numerical modeling. *J Geophys Res* 105:28363–28376
- McCarthy AJ, Elders CF (1997) Cenozoic deformation in Sumatra: oblique subduction and the development of the Sumatran fault system, in Fraser, A. J., Matthews, S. J. & Murphy, R. W. (editors) *Petroleum Geology of Southeast Asia*. Geol Soc Spec Publ 126:355–363
- McNeill LC, Henstock TJ (2014) Forearc structure and morphology along the Sumatra-Andaman subduction zone. *Tectonics*. <https://doi.org/10.1002/2012TC003264>
- Michel GW, Becker M, Angermann D, Reigber C, Reinhart E (2000) Crustal motion in E-and SE-Asia from GPS measurements. *Earth Planets Space* 52:713–720. <https://doi.org/10.1186/BF03352270>
- Michel GW, Yu YQ, Zhu SY, Reigber C, Becker M, Reinhart E, Simons W, Ambrosius B, Vigny C, Chamot-Rooke N, Le Pichon X, Morgan P, Matheussen S (2001) Crustal motion and block behaviour in SE-Asia from GPS measurements. *Earth Planet Sci Lett* 187:239–244
- Minster JB, Jordan TH (1978) Present-day plate motions. *J Geophys Res* 83:5331–5354
- Mitchell AHG (1981) Phanerozoic plate boundaries in mainland SE Asia, The Himalayas and Tibet. *J Geol Soc Lond* 138:109–122
- Mitchell AHG, McKerrow WS (1975) Analogous evolution of the Burma orogen and the Scottish Caledonides. *Geol Soc Am Bull* 86:305–315
- Molnar P, Deng Q (1984) Faulting associated with large earthquakes and the average rate of deformation in central and eastern Asia. *J Geophys Res* 89:6203–6227
- Mookerjee M, Canada A, Fortescue FQ (2016) Quantifying thinning and extrusion associated with an oblique subduction zone: an example from the rosy finch shear zone. *Tectonophysics* 693:290–303
- Morishita T, Soe HM, Htay H, Lwin TH, Guotana JM, Tamura A, Mizukami T, Zaw K (2023) Origin and evolution of ultramafic rocks along the Sagaing fault Myanmar. *J Earth Sci* 34:122–132. <https://doi.org/10.1007/s12583-021-1435-x>
- Morra G, Regenauer-Lieb K, Giardini D (2006) Curvature of oceanic arcs. *Geology* 34:877–880
- Mukhopadhyay B, Dasgupta S, Mukherjee P (2016) Slab tear and tensional fault systems in the Sunda-Andaman Benioff zone: implications on tectonics and potential seismic hazard. *Geomat Nat Haz Risk* 7:1129–1146. <https://doi.org/10.1080/19475705.2015.1011242>
- Mukti MM, Singh SC, Deighton I, Hananto ND, Moeremans R, Permana H (2012) Structural evolution of backthrusting in the Mentawai fault zone, offshore Sumatran forearc. *Geochem Geophys Geosyst* 13:Q12006. <https://doi.org/10.1029/2012GC0004199>
- Munem MA, Foulis DJ (1984) *Calculus with analytic geometry*. Worth Publishers
- Natawidjaja DH (2018) Updating active fault maps and sliprates along the Sumatran fault zone Indonesia. *IOP Conf Series Earth Environ Sci*. <https://doi.org/10.1088/1755-1315/118/1/012001>
- Natawidjaja DH, Sieh K, Chlieh M, Galetzka J, Suwargadi BW, Hai Cheng R, Edwards L, Avouac J-P, Ward SN (2006) Source parameters of the great Sumatran megathrust earthquakes of 1797 and 1833 inferred from coral microatolls: the 1797 and 1833 great Sumatran earthquakes. *J Geophys Res Solid Earth*. <https://doi.org/10.1029/2005JB004025>
- Newcomb KR, McCann WR (1987) Seismic history and seismotectonics of the Sunda arc. *J Geophys Res* 92:421–439
- Ni JF, Guzmán-Speziale M, Bevis M, Holt WE, Wallace T, Seager WR (1989) Accretionary tectonics of Burma and the three-dimensional geometry of the Burma subduction zone. *Geology* 17:68–71
- Panda D, Kundu B, Gahalaut VK, Rangin C (2020) India-Sunda plate motion, crustal deformation, and seismic hazard in the Indo-Burmese Arc. *Tectonics*. <https://doi.org/10.1029/2019TC006034>
- Panda D, Kundu B, Santosh M (2018) Oblique convergence and strain partitioning in the outer deformation front of NE Himalaya. *Sci Rep* 8:10564. <https://doi.org/10.1038/s41598-018-28774-3>
- Philibosian B, Sieh K, Avouac JPh, Natawidjaja DH, Chiang H-W, Wu C-C, Shen C-C, Daryono MR, Perfettini H, Suwargadi BW, Lu Y, Wang X (2017) Earthquake supercycles on the Mentawai segment of the Sunda megathrust in the seventeenth century and earlier. *J Geophys Res* 122:642–676. <https://doi.org/10.1002/2016JB013560>
- Philippon M, Corti G (2016) Obliquity along plate boundaries. *Tectonophysics* 693:171–182
- Platt JP (1993) Mechanics of oblique convergence. *J Geophys Res* 98:16239–16256
- Radha Krishna M, Sanu TD (2002) Shallow seismicity, stress distribution and crustal deformation pattern in the Andaman-west Sunda arc and Andaman sea, Northeastern Indian ocean. *J Seismolog* 6:25–41
- Rafie MT, Sahara DP, Cummins PR, Triyoso W, Widiyantoro S (2023) Stress accumulation and earthquake activity on the great Sumatran fault Indonesia. *Natural Hazards*. <https://doi.org/10.1007/s11069-023-05816-2>
- Rajendran K, Gupta HK (1989) Seismicity and tectonic stress field of a part of the Burma-Andaman-Nicobar arc. *Bull Seismol Soc Am* 79:989–1005. <https://doi.org/10.1785/BSSA0790040989>
- Rangin C (2016) Rigid and non-rigid micro-plates: Philippines and Myanmar-Andaman case studies. *CR Geosci* 348:33–41
- Rodolfo KS (1969) Bathymetry and marine geology of the Andaman basin, and tectonic implications for southeast Asia. *Geol Soc Am Bull* 80:1203–1230
- Sagazan C, Olive J-A (2021) Assessing the impact of sedimentation on fault spacing at the Andaman sea spreading center. *Geology* 49:447–451. <https://doi.org/10.1130/G48263.1>
- Salman R, Lindsey EO, Feng L, Bradley K, Wei S, Wang T, Daryono MR, Hill EM (2020) Structural controls on rupture extent of recent Sumatran fault zone earthquakes, Indonesia. *J Geophys Res Solid Earth*. <https://doi.org/10.1029/2019JB018101>
- Samuel MA, Harbury NA (1996) The Mentawai fault zone and deformation of the Sumatran forearc in the Nias area. *Geol Soc Lond Spec Publ* 106:337–351
- Satyabala SP (1998) Subduction in the Indo-Burma region: Is it still active? *Geophys Res Lett* 25:3189–3192



- Satyabala SP (2003) Oblique plate convergence in the Indo-Burma (Myanmar) Subduction region. *Pure Appl Geophys* 160:1611–1650
- Schellart WP (2004) Kinematics of subduction and subduction-induced flow in the upper mantle. *J Geophys Res* 109:B07401. <https://doi.org/10.1029/2004JB002970>
- Schellart WP, Stegman DR, Farrington RJ, Moresi L (2011) Influence of lateral slab edge distance on plate velocity, trench velocity, and subduction partitioning. *J Geophys Res* 116:B10408. <https://doi.org/10.1029/2011JB008535>
- Schütt JM, Whipp DM (2020) Controls on continental strain partitioning above an oblique subduction zone Northern Andes. *Tectonics* 39:e2019TC005886. <https://doi.org/10.1029/2019TC005886>
- Scotese CR, Rowley DB (1985) The orthogonality of subduction: An empirical rule? *Tectonophysics* 116:173–187
- Seymour NM, Singleton JS, Gomila R, Mavor SP, Heuser G, Arancibia G, Williams S, Stockli DF (2021) Magnitude, timing, and rate of slip along the Atacama fault system, northern Chile: implications for early cretaceous slip partitioning and plate convergence. *J Geol Soc* 178:jgs2020-2142. <https://doi.org/10.1144/jgs2020-142>
- Shamim S, Khan PK, Mohanty SP, Mohanty M (2021) Andaman–Nicobar–Sumatra margin revisited: analysis of the lithospheric structure and deformation based on gravity modeling and distribution of seismicity. *Surv Geophys* 42:239–275. <https://doi.org/10.1007/s10712-021-09633-9>
- Siebert L, Simkin T, Kimberly P (2011) *Volcanoes of the world*. University of California Press, Smithsonian Institution
- Sieh K, Natawidjaja D (2000) Neotectonics of the Sumatran fault, Indonesia. *J Geophys Res* 105:28295–28326
- Simons WJF, Socquet A, Vigny C, Ambrosius BAC, Haji Abu S, Promthong C, Subarya C, Sarsito DA, Matheussen S, Morgan P, Spakman W (2007) A decade of GPS in Southeast Asia: resolving sundaland motion and boundaries. *J Geophys Res* 112:B06420. <https://doi.org/10.1029/2005JB003868>
- Singh LS, Gahalaut VK, Kumar A (2014) Nine years of GPS measurements of crustal deformation at Imphal Indo-Burmese wedge. *J Geol Soc India* 83:513–516
- Singh SC, Hanato ND, Chauhan APS, Permana H, Denolle M, Hendriyana A, Natawidjaja D (2010) Evidence of active backthrusting at the NE Margin of Mentawai Islands SW Sumatra. *Geophys J Int* 180:703–714. <https://doi.org/10.1111/j.1365-246X.2009.04458.x>
- Singh AP, Purnachandra Rao N, Ravi Kumar M, Hsieh M-C, Zhao L (2017) Role of the Kopili fault in deformation tectonics of the Indo-Burmese Arc inferred from the rupture process of the 3 January 2016 Mw 6.7 imphal earthquake. *Bull Seismol Soc Am*. <https://doi.org/10.1785/0120160276>
- Singha P, Dewangan P, Kamesh Raju KA, Aswini KK, Ramakrushana Reddy T (2019) Geometry of the subducting Indian Plate and local seismicity in the Andaman region from the passive OBS experiment. *Bull Seismol Soc Am* 109:797–811. <https://doi.org/10.1785/0120180178>
- Smith WHF, Sandwell DT (1997) Global sea floor topography from satellite altimetry and ship depth soundings. *Science* 277:1956–1962. <https://doi.org/10.1126/science.277.5334.1956>
- Snehashis A, Vijaya SM, Kumar MK, Shoaib R (2022) Characteristics of the earthquake swarms in the Andaman sea region, India, from 1960–2020. *Disaster Adv*. <https://doi.org/10.25303/1503da2128>
- Socquet A, Vigny C, Chamot-Rooke N, Simons W, Rangin C, Ambrosius B (2006) India and Sunda plates motion and deformation along their boundary in Myanmar determined by GPS. *J Geophys Res* 111:B05406. <https://doi.org/10.1029/2005JB003877>
- Srijayanthi G, Ravi Kumar M, Prasanna S, Purnachandra Ran N (2017) Source characteristics of the 2012 earthquake swarm activity in the Andaman spreading ridge. *J Indian Geophys Union* 21:25–33
- Srijayanthi G, Ravi Kumar M (2020) Seismicity, lithospheric structure and mantle deformation in the Andaman Nicobar subduction zone. In: Ray JS, Radhakrishna M (eds) *The Andaman Islands and adjoining offshore: geology, tectonics and palaeoclimate*. Springer, Cham, pp 107–136
- Srivastava N, Köhler J, Nava FA, El Sayed O, Chakraborty M, Steinheimer J, Faber J, Kies A, Thingbaijam KK, Zhou K, Rumpker G, Stoecker H (2021) Sunda Arc seismicity: continuing increase of high-magnitude earthquakes since 2004. *arXiv Preprint arXiv:2108.06557*
- Stanton-Yonge A, Griffith WA, Cembrano J, Julien RS, Iturrieta P (2016) Tectonic role of margin-parallel and margin-transverse faults during oblique subduction in the southern volcanic zone of the Andes: insights from boundary element modeling. *Tectonics* 35:1990–2013. <https://doi.org/10.1002/2016TC004226>
- Steckler MS, Mondal DR, Akhter SH, Seeber L, Feng L, Gale J, Hill EM, Howe M (2016) Locked and loading megathrust linked to active subduction beneath the Indo-Burman ranges. *Nat Geosci* 9:615–619. <https://doi.org/10.1038/NNGEO2760>
- Sukmono S, Zen MT, Hendrajaya L, Kadir WGA, Santoso D, Dubois J (1997) Fractal pattern of the Sumatra fault seismicity and its possible application to earthquake prediction. *Bull Seismol Soc Am* 87:1685–1690
- Syafriani S (2018) An investigation of seismicity for the West Sumatra region Indonesia. *IOP Conf Series Mater Sci Eng* 335:012009
- Teyssier C, Tikoff B, Markley M (1995) Oblique plate motion and continental tectonics. *Geology* 23(447):450
- Tin TZH, Nishimura T, Hashimoto M, Lindsey EO, Aung LT, Min SM, Thant M (2022) Present-day crustal deformation and slip rate along the southern Sagaing fault in Myanmar by GNSS observation. *J Asian Earth Sci* 228:105125. <https://doi.org/10.1016/j.jseae.2022.105125>
- Tiwari RP, Gahalaut VK, Rao ChUB, Lalsawta C, Kundu B, Mal-sawmtluanga, (2015) No evidence for shallow shear motion on the Mat fault, a prominent strike slip fault in the Indo-Burmese wedge. *J Earth Syst Sci* 124:1039–1046
- Toda S, Kaneda H, Okada S, Ishimura D, Mildon ZK (2016) Slip-partitioned surface ruptures for the Mw 7.0 16 April 2016 Kumamoto, Japan, earthquake. *Earth Planets Space*. <https://doi.org/10.1186/s40623-016-0560-8>
- Tovish A, Schubert G (1978) Island arc curvature, velocity of convergence and angle of subduction. *Geophys Res Lett* 5:329–332
- Tozer B, Sandwell DT, Smith WHF, Olson C, Beale JR, Wesel P (2019) Global bathymetry and topography at 15 arc sec: SRTM15+. *Earth Space Science* 6:1847–1864. <https://doi.org/10.1029/2019EA000658>
- Tsutsumi H, Sato T (2009) Tectonic geomorphology of the southernmost Sagaing fault and surface rupture associated with the May 1930 Pegu (Bago) earthquake Myanmar. *Bull Seismol Soc Am* 99:2155–2168. <https://doi.org/10.1785/0120080113>
- Vigny C, Socquet A, Rangin C, Chamot-Rooke N, Puebellier M, Bouin M-N, Bertrand G, Becker M (2003) Present-day crustal deformation around Sagaing fault, Myanmar. *J Geophys Res* 108:2533. <https://doi.org/10.1029/2002JB001999>
- Wang Y, Gao Y, Morley CK, Seagreen EG, Qian X, Rimando JM, Zhang P, Wang Y (2023) Pleistocene accelerated exhumation within the Sumatran fault: implications for late cenozoic evolution of Sumatra (Indonesia). *Geophys Res Lett*. <https://doi.org/10.1029/2022GL100028>
- Weller O, Lange D, Tilmann F, Natawidjaja D, Rietbrock A, Collings R, Gregory L (2012) The structure of the Sumatran fault revealed by local seismicity. *Geophys Res Lett* 39:L01306. <https://doi.org/10.1029/2011GL050440>
- Wessel P, Smith WHF (1991) Free software helps map and display data. *EOS Trans Am Geophys Union* 72:441



- Wessel P, Smith WHF (1995) New version of the generic mapping tools released. *EOS Trans Am Geophys Union* 76:329
- Wessel P, Smith WHF (1998) New, improved version of the generic mapping tools released. *EOS Trans Am Geophys Union* 79:579
- Wessel P, Smith WHF, Scharro R, Luis JF, Wobbe F (2013) Generic mapping tools: improved version released. *EOS Trans Am Geophys Union* 94:409–410
- Weston J, Engdahl ER, Harris J, di Giacomo D, Storchack DA (2018) ISC-EHB: Reconstruction of a robust earthquake dataset. *Geophys J Int* 214:474–484. <https://doi.org/10.1093/gji/ggy155>
- Wiens DA, DeMets C, Gordon RG, Stein S, Argus D, Engeln JF, Lundgren P, Quible D, Stein C, Weinstein S, Woods DF (1985) A diffuse plate boundary model for Indian ocean tectonics. *Geophys Res Lett* 12:429–432
- Yamaoka K, Fukao Y (1987) Why do island arcs form cusps at their junctions? *Geology* 15:34–36
- Yamaoka K, Fukao Y, Kumazawa M (1986) Spherical shell tectonics: effects of sphericity and inextensibility on the geometry of the descending lithosphere. *Rev Geophys* 24:27–53
- Zhang R, Jiang S-Y, Donelick RA, Li R, Soares CJ, Mei L (2022a) Frontal expansion of an accretionary wedge under highly oblique plate convergence: southern Indo-Burman ranges Myanmar. *Geol Soc Am Bull.* <https://doi.org/10.1130/B36560.1>
- Zhang R, Li S, Suo Y, Liu J, Cao X, Zhou J, Jiang Z, Li X (2022b) A forearc pull-apart basin under oblique arc-continent collision: insights from the North Luzon trough. *Tectonophysics* 837:229461. <https://doi.org/10.1016/j.tecto.2022.229461>